



HAL
open science

Inferring channel incision in gravel-bed rivers: Integrating LiDAR data, historical aerial photographs and drone-based SfM topo-bathymetry

Miloš Rusnák, Ján Kaňuk, Anna Kidová, Milan Lehotský, Hervé Piégay, Ján Sládek, Lukáš Michaleje

► To cite this version:

Miloš Rusnák, Ján Kaňuk, Anna Kidová, Milan Lehotský, Hervé Piégay, et al.. Inferring channel incision in gravel-bed rivers: Integrating LiDAR data, historical aerial photographs and drone-based SfM topo-bathymetry. *Earth Surface Processes and Landforms*, 2024, 49 (8), pp.2475-2497. 10.1002/esp.5840 . hal-04803937

HAL Id: hal-04803937

<https://hal.science/hal-04803937v1>



Submitted on 26 Nov 2024

HAL is a multi-disciplinary open access archive for the deposit and dissemination of scientific research documents, whether they are published or not. The documents may come from teaching and research institutions in France or abroad, or from public or private research centers.

L'archive ouverte pluridisciplinaire **HAL**, est destinée au dépôt et à la diffusion de documents scientifiques de niveau recherche, publiés ou non, émanant des établissements d'enseignement et de recherche français ou étrangers, des laboratoires publics ou privés.

RESEARCH ARTICLE

Inferring channel incision in gravel-bed rivers: Integrating LiDAR data, historical aerial photographs and drone-based SfM topo-bathymetry

Miloš Rusnák¹  | Ján Kaňuk² | Anna Kidová¹ | Milan Lehotský¹ |
Hervé Piégay³  | Ján Sládek¹ | Lukáš Michaleje¹

¹Department of Physical Geography, Geomorphology and Natural Hazards, Institute of Geography, Slovak Academy of Sciences, Bratislava, Slovakia

²Institute of Geography, Faculty of Science, Pavol Jozef Šafárik University in Košice, Košice, Slovakia

³University of Lyon, UMR 5600 Environnement Ville Société, CNRS, Site of ENS Lyon, Lyon, France

Correspondence

Miloš Rusnák, Department of Physical Geography, Geomorphology and Natural Hazards, Institute of Geography, Slovak Academy of Sciences, Štefánikova 49, 814 73 Bratislava, Slovakia.
Email: geogmilo@savba.sk

Funding information

Vedecká Grantová Agentúra MŠVVaŠ SR a SAV, Grant/Award Numbers: 01/0085/23, 02/0016/24; Graduate School H2O'Lon, Grant/Award Number: ANR-17-EURE-0018

Abstract

Channel incision is an evident trend for river evolution in many European rivers and notably the Western Carpathians, whose former braided and multichannel wandering river system is transforming into a single-thread channel, but it is often difficult to separate drivers and determine if incision is finished or is still ongoing. To overpass these research gaps, this paper presents an innovative approach to assess the multidecadal incision of the Belá River in the Western Carpathians since 1949 by LiDAR-based analyses of floodplain surfaces above the river channel dated from historical aerial images. Detailed analyses of ongoing incision were also calculated based on DEM of differences (DoD) using Structure-from-Motion (SfM) photogrammetry-derived topo-bathymetric models. The study applied the BACI (Before-After-Control-Impact) approach that compared *pre-state* (Before), *post-state* (After) and reach (*Control*) that is not affected by potential external effects with degraded (impacted) reach to be able to distinguish the driver effects. Floodplain channel surface analyses indicate the maximum incision up to 4 m and incision rate of 5.7 cm/year that occurred in the most degraded reach. Moreover, cross-section profiles point to accelerated incision of 24.5 cm/year in the last 10 years (2011–2021) by the propagation of incision upstream. Overall, the net changes from the UAV survey pointed to 22 759 m³ of gravel sediments, constituting outwash from the 1.6 km long channel system (2015–2022) by incision, whereas analyses of historical channel surfaces estimated erosion of 573 303 m³ from impacted reaches between 1949 and 2020. Incision evidence is only observed in the downstream part below the control section due to local drivers (channel regulation, comprising embankment and gravel mining that activated a backward erosion of the system with knickpoint migration upstream). This analysis shows the benefits of combining different sources of data to separate long-term and ongoing channel responses and the BACI-approach to better target cause–effect relationships in space and time.

KEYWORDS

bathymetry, Carpathian rivers, DoD, human impact, incision, SfM-photogrammetry

1 | INTRODUCTION

In Europe, river systems have been significantly affected by narrowing and channel planform transformation due to changes in natural conditions and increased human pressure on the landscape. Anthropogenic

modifications, grade-control structures and channelisation have led to active channel narrowing, planform transformation and bed incision (Brierley & Mum, 1997; Gorczyca et al., 2020; James, 1997; Kidová et al., 2021; Klimek, 1987; Liébault & Piégay, 2002; Perçoiu & Rădoane, 2011; Rădoane et al., 2013; Scorpio et al., 2018; Škarpich

et al., 2013; Škarpich, Kašpárek, et al., 2016; Wyźga, Zawiejska, & Hajdukiewicz, 2016; Zawiejska & Wyźga, 2010; Ziliani & Surian, 2012). Channel degradation is primarily associated with transformations in sediment availability in the catchment (Liébault & Piégay, 2002) by its decreases due to factors like gravel extraction (Marston et al., 2003; Rinaldi et al., 2005; Surian & Rinaldi, 2003), channelisation (Hajdukiewicz et al., 2017; Korpak, 2007; Scorpio et al., 2018), dam construction (Surian, 1999) or land cover changes such as afforestation (Jefferson & McGee, 2013; Liébault et al., 2005; Price & Leigh, 2006).

Channel incision is a critical issue on European rivers, often linked to channel narrowing and transformation of former braided channels into a single-thread and multithread wandering river system (see examples and detailed information about incision in the Supporting Information section S1). Lowering of streambed elevation is caused by erosion due to imbalances between sediment transport capacity and sediment supply into the channel (Simon & Rinaldi, 2006). Human impact is detected as a major driver causing channel incision.

Generally, studies of long-term channel incision are primarily focused on the analyses of historical geodetic profiles from topographic or hydrometric surveys (Table 1). Channel bed elevation lowering is detected by contrasting historical longitudinal and cross-sectional profiles with present channel conditions (Arnaud et al., 2015; Dufour & Piégay, 2010; Ferrer-Boix et al., 2023; James, 1991; Kondolf et al., 2002; Škarpich et al., 2013, 2020; Surian et al., 2009; Wyźga, 2001). As indirect approaches, are used informations from lowering the annual minimum water level, following condition that the channel width remains constant over time (Chiriloaei et al., 2012; Hajdukiewicz et al., 2017; Rădoane et al., 2013; Wyźga, 1991, 1993, 2001) or historical photographs of undercutting bridges are compared (Galay, 1983; Kondolf & Swanson, 1993; Ferrer-Boix et al., 2023). The problem arises when historical data are not available, or the incision is not detectable from photographs or minimum water level measurements. Several indirect approaches are used for the identification of bed lowering. Incision rate can be assumed from differences between actual riverbeds and a theoretical profile or models (Rovira et al., 2005). Comparison of the vertical position of fluvial geomorphic landforms above floodplain that is measured by RTK-GNSS and dated by aerial images is used in paper by Calle et al. (2017). Liébault and Piégay (2002) measured the height of the abandoned side channels above the present bed position from floodplain cross-section. Absence of historical information can be substituted by old topographic map with elevation data (Armaş et al., 2013) and historical aerial photographs that can be 3D photogrammetrically processed from stereo pairs (Hajdukiewicz et al., 2019; Llana et al., 2020).

Moreover, point clouds serve as valuable resources for topographic analyses and identification of channel transformation (Bertoldi et al., 2011; Bizzi et al., 2019; Heritage & Hetherington, 2007). Time series of LiDAR (light detection and ranging) datasets allow the calculation of volumetric changes by subtracting digital elevation models (DEMs), facilitating the identification of lateral erosion, sediment deposition or vertical incisions with high accuracy and precision (Croke et al., 2013; Lallias-Tacon et al., 2017; Wheaton et al., 2009). LiDAR elevation models also include details about the evolution of historical floodplains. In recent years, the development of low-cost monitoring through unmanned aerial vehicles (UAVs) and the

TABLE 1 Summary of different methods that are used for identification of the vertical change of bed level of selected rivers (examples and detailed information about incision in the Supporting Information section S1).

Methods	References
Historical cross-section survey	Arnaud et al., 2015; Galay, 1983; James, 1991, 1997; Kondolf & Swanson, 1993; Llana et al., 2020; Peiry, 1987; Rădoane et al., 2010; Rinaldi & Simon, 1998; Surian & Cisotto, 2007; Surian & Rinaldi, 2003; Škarpich et al., 2013, 2020
Historical longitudinal profiles	Dufour & Piégay, 2010; Ferrer-Boix et al., 2023; James, 1991; Kondolf et al., 2002; Lach & Wyźga, 2002; Liébault & Piégay, 2002; Martín-Vide et al., 2010; Petit et al., 1996; Rinaldi, 2003; Rinaldi & Simon, 1998; Škarpich, Galia, & Hradecký, 2016
Lowering of minimum annual water stages at gauging stations	Chiriloaei et al., 2012; Hajdukiewicz et al., 2017; James, 1991; Korpak, 2007; Lach & Wyźga, 2002; Rădoane et al., 2013; Wiejaczka & Kijowska-Strugała, 2015; Wyźga, 1991, 1993, 2001; Wyźga, Zawiejska, & Hajdukiewicz, 2016
Historical longitudinal profiles and cross-section survey	Surian et al. (2009)
Bridges undercutting	Ferrer-Boix et al., 2023; Galay, 1983; Kondolf & Swanson, 1993
3D photogrammetrically processed aerial images	Hajdukiewicz et al., 2019; Llana et al., 2020
Longitudinal profile from a topographic map and present cross-section survey	Armaş et al., 2013
Hanging gravels measured by RTK-GPS (dating by aerial photos)	Calle et al., 2017
Cross-section (floodplain vertical changes)	Liébault & Piégay, 2002
Differences between an actual riverbed and a theoretical profile	Rovira et al., 2005

application of Structure-from-Motion (SfM) photogrammetry (Fonstad et al., 2013; James & Robson, 2012) have opened new avenues for detecting high-resolution topographic changes in river systems (Calle et al., 2018, 2020; Marteau et al., 2017, 2020; Miříjovský & Langhammer, 2015). In GIS software, these new 3D data are easy to compare with historical aerial images with information about horizontal channel adjustment, long-term planform analyses and transformations of active channel width (Bertalan et al., 2019; Greco et al., 2007; Hajdukiewicz & Wyźga, 2022; Kidová et al., 2016; Liro, 2015; Llana et al., 2020; Marchese et al., 2017; Michalková et al., 2011; Ollero, 2010; Scorpio et al., 2015; Surian & Rinaldi, 2003).

In degraded river reaches, questions linger about how incision will evolve in the future. Additionally, there is uncertainty on how one can implement management strategies to prevent channel degradation, stabilise the transformation under the system's new conditions or restore the morphological state. Previous studies focus primarily on the actual state and description of the past events, concentrating on the single reach without differentiating the control and impact sections. Generally, the BACI (Before-After-Control-Impact) approach is developed for understanding the effect of revitalisation, but it is applicable for understanding the impact of any drivers or changes in the river channel (Bulteau et al., 2022). Separation of upstream and downstream controls, and local and catchment controls based on a multi-BACI approach, is still lacking and challenging for understanding river incision. This paper aims to analyse the incision rate in the river system without historical data. We apply new emerging technology to date incision based on narrowing, as shown by Lallias-Tacon et al. (2017). This approach was supplemented by intensive UAV monitoring to go further and consider ongoing incision based on SfM-photogrammetry and calculation incision budgeting. Finally, we aim to deepen the understanding of channel degradation by

- i. evaluating long-term channel pattern alterations in a multithread channel system from 1949;
- ii. identifying channel incisions by calculating the historical rate of incision over an extended period from 1949, using an innovative approach rooted in floodplain spatial memory;
- iii. quantifying the sediment deficit and incision budgeting for the period 1949–2020;
- iv. determining the primary driving forces behind channel transformation by using the BACI approach and separate upstream and local controls on channel incision.

2 | STUDY RIVER

The Belá River flows in northern Slovakia with a length of 23.6 km, exhibiting a multithread planform (as documented by Kidová et al., 2016, 2017) and braidplain width averages between 18 and 126 m. Originating from the slopes of the Western and High Tatra Mountains and reaching an elevation of 627 m a.s.l. up to 2494 m a.s.l. The catchment area spans 244 km². The river is predominantly fed by right-bank, high-energy tributaries from the Western Tatras, as depicted in Figure 1. From a geomorphological perspective, the northern part of the catchment belongs to the Tatra Mountains and primarily consists of pre-Mesozoic crystalline rocks (specifically granitoid complex) and autochthonous Permian-Mesozoic sequences (Nemčok et al., 1994). The southern part, the Liptovská kotlina Basin, is formed by the Inner-Carpathian Paleogene sequences (Gross et al., 1979) with alternation between sandstone and claystone. Layered above these foundational strata are diverse glaciofluvial deposits (outwash) dating back to the Pleistocene glaciation, remnants of the Tatra Mountain's glacial activity. The Holocene floodplain comprises boulders, gravel and gravel-sandy fluvial deposits reaching a thickness of up to 2 m. Notably, these deposits possess an average grain size diameter (d_{50}) of 126 mm (Rusnák et al., 2020).

The hydrological regime is predominantly shaped by snow melting during spring season, leading to moderate-magnitude flood events.

Additionally, the summer season often witnesses heavy rainfalls in mountainous areas, triggering significant floods. Precipitation rates vary across the region. In the lower reaches of the river, annual average precipitation is around 680 mm, whereas in the Tatras, it can escalate to as much as 2000 mm. The mean annual discharge, for the period of records 1964–2006, at Podbanské gauging station is 3.5 m³·s⁻¹. Conversely, the Liptovský Hrádok gauging station has an average annual discharge of 6.8 m³·s⁻¹, as noted by Majerčáková et al. (2007). Flood events were evaluated from the Slovak Hydrometeorological Institute data as well as official flood reports that pointed to the higher magnitude flood events at the beginning of the 20th century, as visually represented in Figure 2.

Throughout the 20th century, the Belá River underwent considerable human-induced changes. At the beginning of the century, grazing and pasture activities predominantly characterised the upper catchment areas. However, this changed post-1949 with the establishment of the Tatras National Park. This led to significant afforestation, especially in the middle and higher altitudes. As a result, forest cover within the catchment increased from 55.4 km² in 1949 to 84.9 km² by 2008 (Kidová et al., 2016). Additionally, the river's lower section underwent channel modifications by the construction of five water mills during the first half of the 20th century. From 1950 onwards, human intervention became more prominent with the initiation of channelisation and embankment works (started in 1938 and ended before aerial imaging in 1961). Another major alteration was the establishment of five small hydropower plants between 1941 and 2000. Interestingly, these plants were constructed in the abandoned old side arms, which were repurposed as headrace channels.

3 | METHODS

3.1 | BACI approach and river sections

For understanding and assessment of the effect of different drivers on channel incision, we select the BACI approach that compared *pre-state* (Before), *post-state* (After) and reach (*Control*) that is not affected by potential external effects. The method was applied for assessment restoration (Marteau et al., 2022) but is applicable for assessing any impacted river system with the different spatial manifestations of channel transformation (Bulteau et al., 2022). The Before-After approach (time scale) is related to the pre-state situation in 1949 and before the main channelisation works that started in the 1950s. This initial state was validated with an old cadastre map from 1866 (Figure 3). Post-state (after 1949) period captured a transformation of the system after external impacts that are represented by catchment scale transformation and local channelisation works. The Control-Impact approach (spatial scale) is applied to the selection of the impacted section with the presence of rapid incision and control (non-impacted by incision) section upstream. This enables the identification of external driving forces effects on spatial scale. Incision evidence only in the downstream part (below the control section) pointed to the local drivers affecting bed lowering, whereas catchment scale factors should affect both control and impacted sections.

The present study focuses on a 9.1-km-long downstream reach of the Belá with varying intensities of human interventions (Figure 1c).

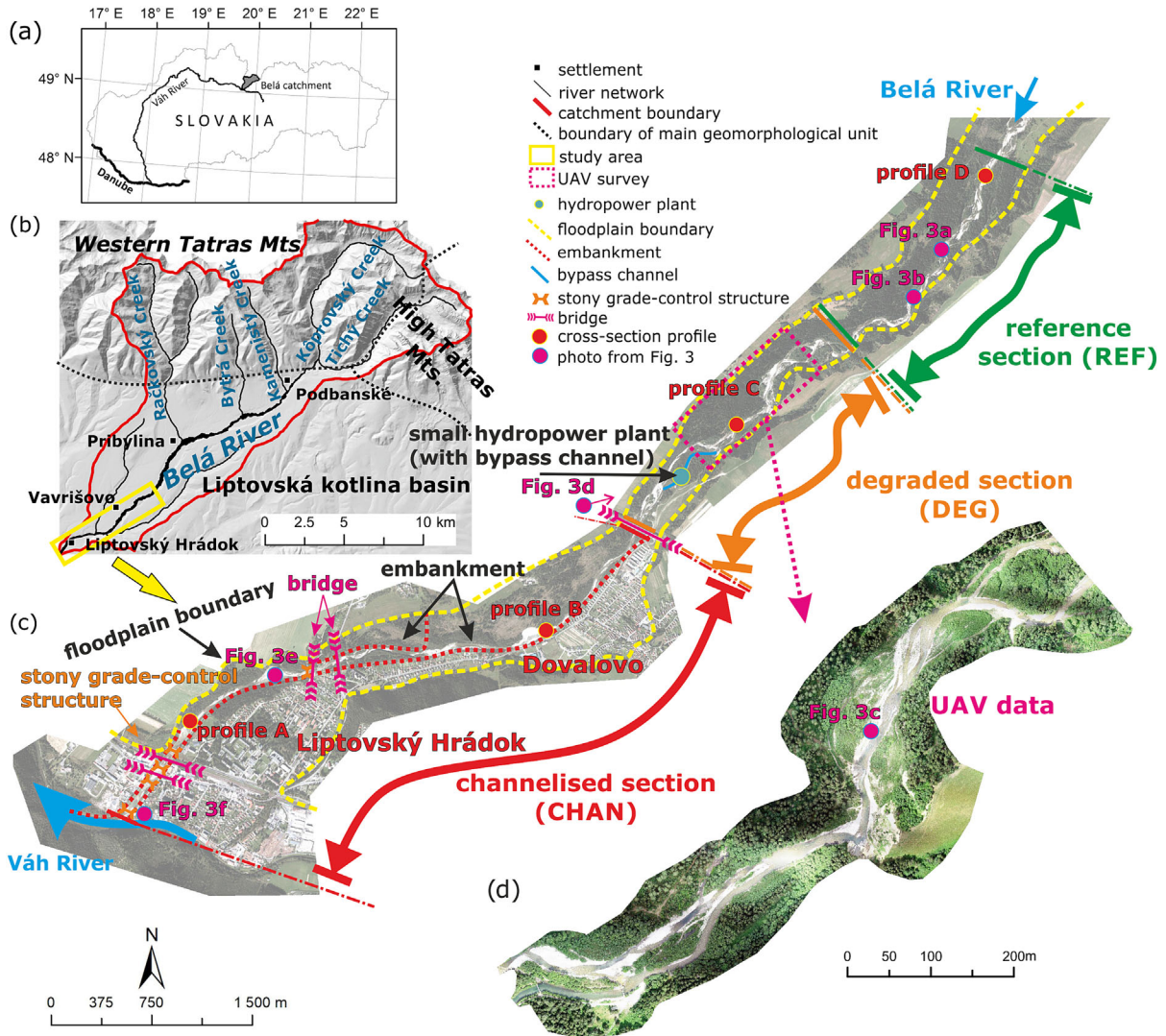


FIGURE 1 General location (a) of the Belá River catchment as a right tributary of the Váh River; (b) catchment area of the Belá River, including the mountainous area in higher parts (Tatra Mountains) with high-energy tributaries, main flow in the Liptovská kotlina Basin and study area near the confluence with the Váh River (yellow rectangle); (c) detailed situation from an aerial photograph, depicting the main anthropogenic intervention, the locations of the three different river sections studied here (CHAN, DEG and REF) and the locations of the UAV data collection sites (purple rectangle); (d) detail of UAV survey area in DEG section.

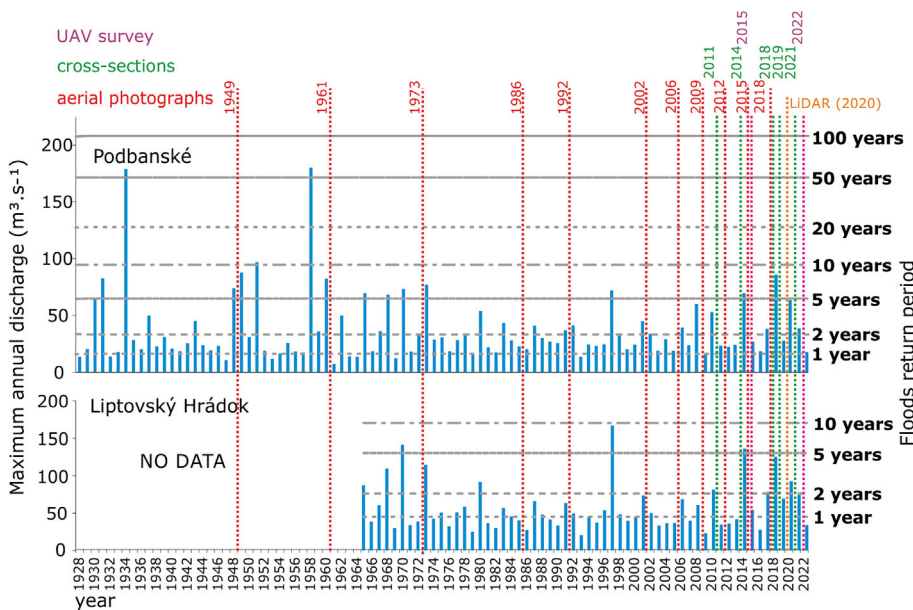


FIGURE 2 Flow series of maximal annual discharges at the Podbanské and Liptovský Hrádok gauging station with flood return period and time horizons of data acquisition (aerial photographs, cross-section profiles, UAV survey and LiDAR data).

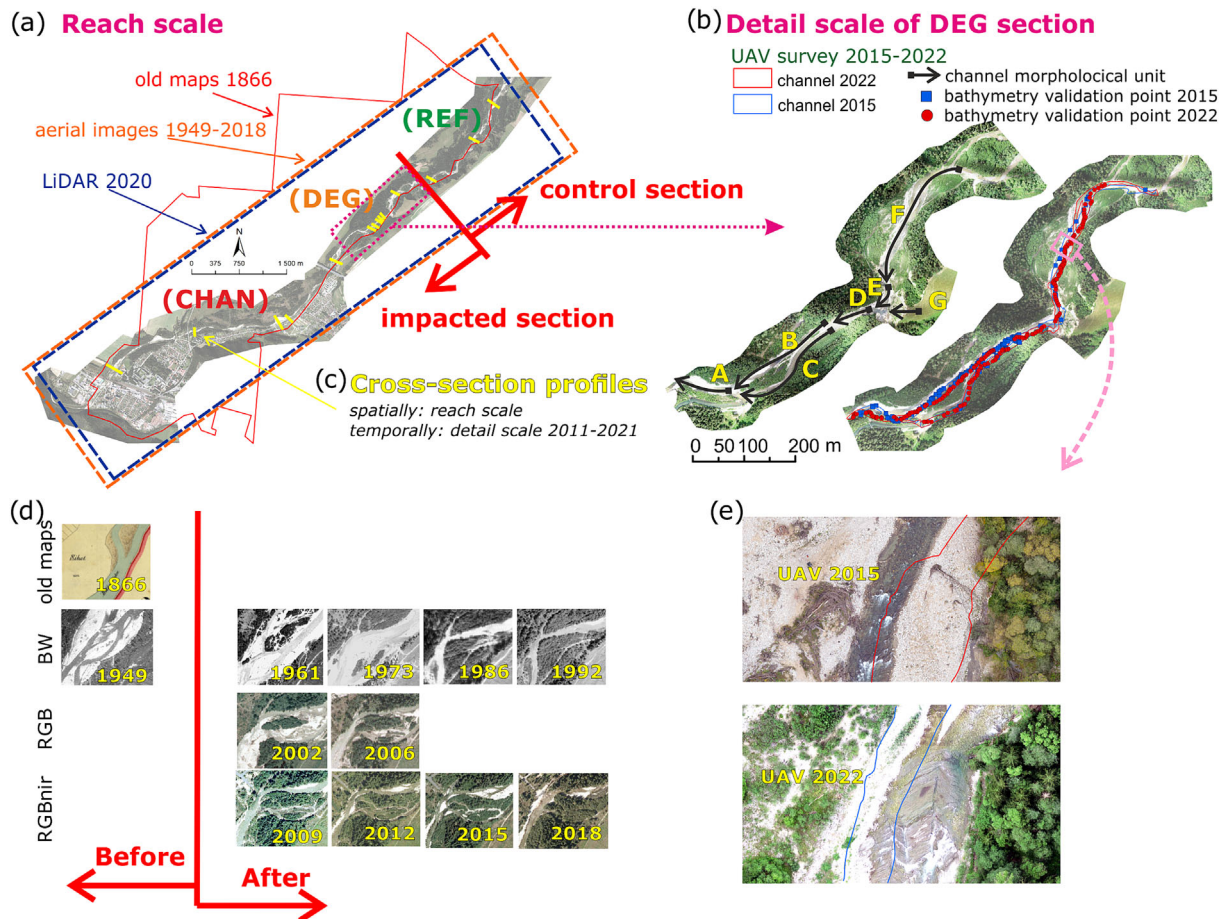


FIGURE 3 Spatial extent of datasets and BACI (Before-After-Control-Impacted) approach that was used for reach scale analysis (a); application of UAV survey for detailed analyses of DEG section (b); and location of cross-section profiles for incision validation in the period 2011–2021 (c). Temporal analyses of before and after state (d) and detail to head-cut evolution in DEG section from UAV survey (e).

This part of the river was divided based on the field works into control non-impacted section (REF) and two impacted sections (DEG and CHAN) downstream from the control one.

The control (REF) section, specifically a 2.1-km-long stretch of the river, remains untouched by direct human intervention (Figure 4a,b). It is characterised as a multichannel gravel-bed section with significant lateral mobility, preserving all natural processes. Bank heights in this area range from 30 to 120 cm, allowing for channel avulsion to the floodplain following gravel deposition during floods. There is no observable evidence of channel incision in this section, and the sediment transport is adequate to support the lateral dynamics and the reworking of the gravel-bed planform. The position of the REF section upstream from the impacted section enables the separation of the effect upstream (catchment) controls from the local ones that are responsible for channel incision in downstream sections.

The second river reach (DEG—degraded section) represents the impacted knickpoint zone (Figure 1d) downstream from the control section and exhibits clear signs of channel incision (Figure 4c,d). This section measures 2.1 km in length. In the middle of the 20th century, this river reach was characterised by a wide braidplain and multi-channel planform that was transformed into a wandering system. In 2000, a small hydropower plant was built on the location of an old abandoned channel. Presently, a secondary channel provides a water supply to a hydropower plant and is artificially maintained using heavy machinery to ensure a water connection to the plant.

The channelised (CHAN) section, extending from the confluence with the Váh River to the highway bridge, spans 4.9 km. The river flows through two urbanised areas, Liptovský Hrádok and Dovalovo (Figure 4e,f) and is fully embanked on the left bank and partially on the right. Near the confluence, five stony grade-control structures were built in the 1990s to protect the road and railway bridges from undercutting. Furthermore, between 1950 and 2000, an estimated 140 000 m³ of gravel was extracted from this section (Kidová et al., 2016). Here, the river creates a sinuous channel with alternate gravel bars.

3.2 | Data sources

3.2.1 | Aerial photos and historical maps

Aerial photographs and orthophotos from 1949, 1961, 1973, 1981, 1992, 2002, 2006, 2009, 2012, 2015 and 2018 were utilised for a long-term historical analysis of channel transformation and planform evolution. Black and white historical images, spanning from 1949 to 1992 (across five-time horizons), were photogrammetrically orthorectified using the ERADS Imagine LPS software (detailed technical information can be found in Supporting Information section S2). These images achieved a final resolution of up to 0.5 m with a root mean square error (RMSE) below 0.5 m for each year. For the time

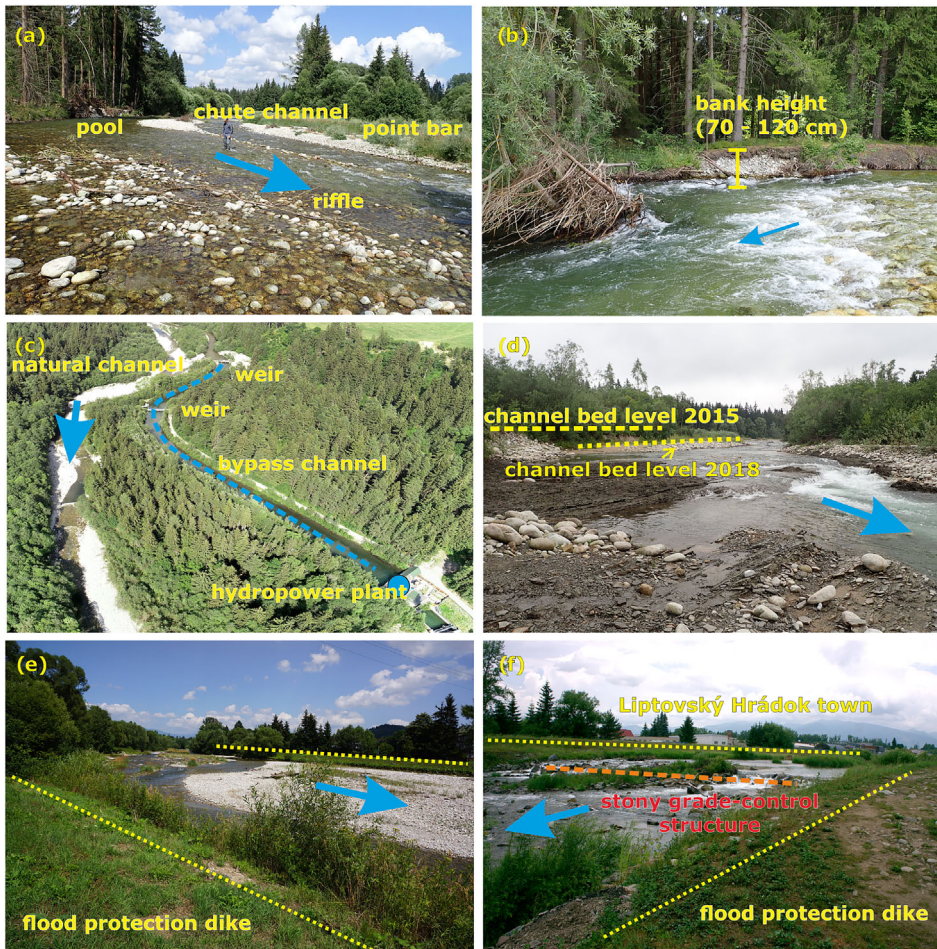


FIGURE 4 Views of different sections of the Belá River; a natural reference section (REF) with active lateral dynamics and in-channel processes (a); without evidence of incision (b); degradation section (DEG) with a headrace canal and a small hydropower plant (c); rapid incision of 1.5 m in the past 10 years (d); the channelised section (CHAN, e); flood protection dikes and stony grade-control structures (f) (for the location of the photo, see Figure 1).

frame beginning in 2002 and spanning six horizons, digital colour orthophotographs with resolutions ranging from 0.5 to 0.2 m were used. Additionally, historical cadastre maps from 1866 were used to determine the channel's position and state in the 19th century. Although these historical maps do not encompass the entire study area, they facilitated the partial reconstruction of the channel's position for approximately 65%–70% of the river's length. Owing to these limitations, these maps were used only for validation of channel incision before 1949 and dating the period when the incision started.

3.2.2 | LiDAR data

LiDAR data were supplied by the Geodesy, Cartography and Cadastre Authority of the Slovak Republic in the form of a LAZ point cloud. These data were captured between 19th November 2019 and 8th April 2020, reaching a vertical accuracy of 0.03 m and an average density for the last reflective points of 18 points/m². The LAStools software was employed for data processing, filtering and ground classification. Only ground points were utilised to generate a digital terrain model (DTM) with a resolution of 0.5 m. Ground DTM was then used to produce a detrended DTM (Williams et al., 2014). Namely, the river's flow path (centerline) was vectorised directly from the DTM and height from the DTM was extracted to centerline vertices, which was subsequently extrapolated as a linear trend surface. The detrended DTM (dedDEM) was constructed by subtracting the linear flow path trend from the original DTM and representing the floodplain elevation above the channel.

3.2.3 | UAV survey

Detailed analyses were conducted on the 1.6-km-long DEG section of the Belá River (Figure 3b) in both 2015 and 2022. In the 2015 campaign, a HiSystem Hexakopter XL equipped with a Sony NEX 6 camera and 16- to 50-mm lens was utilised (Rusnák, Sládek, & Kidová, 2018; Rusnák, Sládek, Kidová, & Lehotský, 2018). A total of 38 ground control points (GCPs) were identified using real-time kinematics (RTK) measurement with GNSS (global navigation satellite system), achieving a positional and vertical accuracy of 1–2 cm (see Table 2 for details). UAV images were captured at above ground level (AGL) of 80, 50 and 20 m, including nadir, oblique and horizontal perspectives. Agisoft Metashape software processes the 1866 aerial images, incorporating 20 of the GCPs in the S-JTSK national coordinates system (the unified trigonometric cadastral network; EPSG:5514), while the remaining 18 GCPs functioned as checkpoints for an accuracy assessment (Table 3). The output from PhotoScan included orthophotomosaics with a resolution of 5 cm and a point cloud with a density ranging between 100 and 200 points per square metre.

The subsequent campaign was performed on 30th June 2022 using a DJI Phantom Pro4 equipped with FC6310 (8.8 mm) camera. For this session, 36 GCPs in the S-JTSK coordinate system were measured with RTK. The UAV flew at heights of 112 and 70 m above the channel, and both nadir and oblique imaging were captured to enhance the geometric quality of the final model. Agisoft Metashape software processed the collection of 2333 images, utilising 14 GCPs and 22 checkpoints, for accuracy verification. To validate the model,

TABLE 2 Basic parameters of UAV flights.

Year	Date	No. images	Camera	AGL (m)	GSD (cm/px)	No. GCP	No. CP
2015	22 Oct.	1866	SONY NEX 6 (16–50 mm)	80, 50, 20	2.38	20	18
2022	30 June	2333	FC6310 (8.8 mm)	112, 70	3.07	14	22

TABLE 3 Processing errors from ground control points (GCP) and checkpoints (CP).

		2015				2022			
		ME	SDE	MAE	RMSE	ME	SDE	MAE	RMSE
GCP	x	−0.0030	0.0192	0.0003	0.0178	0.0000	0.0115	0.0001	0.0105
	y	−0.0015	0.0222	0.0005	0.0213	0.0000	0.0073	0.0000	0.0055
	z	−0.0013	0.0106	0.0001	0.0088	0.0000	0.0078	0.0000	0.0061
CP	x	0.0011	0.0323	0.0011	0.0324	0.0004	0.0206	0.0004	0.0199
	y	0.0010	0.0315	0.0010	0.0315	0.0004	0.0195	0.0004	0.0203
	z	0.0055	0.0135	0.0002	0.0145	0.0278	0.0559	0.0382	0.0608

the various metrics were calculated, including the mean error (ME), the standard deviation error (SDE), the mean absolute error (MAE) and the RMSE. The end results comprised a classified point cloud with a density of 357 points/m² and orthophotomosaic at a resolution of 5 cm.

3.2.4 | Channel cross-section profiles

Channel incision was validated using cross-sectional profiles. Between 2011 and 2021, a total of 14 cross-sectional profiles were measured: four in the CHAN section, seven in DEG and three in the REF section. The average point density in profile transects ranged from approximately 0.5 to 1 per meter of profile length. In 2011 and 2014, measurements were taken using a Leica TCR 307 total station and LaserTech Trupulse 360B laser distance meter, with accuracy variations up to 29.2 mm in elevation. From the 2018 field survey, a GNSS device equipped with RTK positioning was used. This device allowed for mapping with a positional and vertical accuracy of 2 cm. Field campaigns to measure these cross-sectional profiles were conducted in 2011, 2014, 2018, 2019 and 2021. The rate of vertical erosion per year was calculated by dividing differences in elevation of the lowest point of cross-section by the number of years between measurements.

3.3 | DEM construction from UAV

3.3.1 | Generation of dry area

Elevation models derived from the UAV survey were separately generated for dry and wet areas. For DEM generation, a point cloud from the UAV survey was semiautomatically classified to the ground using the Agisoft classification procedure. Subsequently, the model was manually inspected and reclassified in a 3D profile view.

For dry areas, vegetation and wetted channels were masked across both surveys (from the 2015- and 2022-point clouds) based on manual vectorisation. The dry area model was created only for a

part of the river section outside the vegetation mask and wetted channel. Topography of the channel banks in direct contact with the water areas that were overgrown by overhanging vegetation was identified based on the manual classified UAV-SfM ground point clouds. Application of different flight heights with oblique and horizontal images enables the reconstruction of bank topography under vegetation canopy. Individual errors and misclassifications at this water-bank contact point cloud were corrected. In regions with sparser ground point density, linear interpolation was employed to generate a continuous surface. Only ground-classified point cloud from UAV-SfM photogrammetry was converted into a raster with a 10-cm resolution.

3.3.2 | Generation of channel bathymetry

The multiview refraction correction method was used to detect the submerged bed topography, utilising the pyBathySfM software (Dietrich, 2017; Woodget et al., 2019). Point clouds derived from the UAV survey were adjusted through a refraction correction of the cloud points, based on the camera positions. A critical aspect of this procedure is the detection of the water surface, considered as a planar surface connecting both banks. For both data sets, bank lines were vectorised using a detailed UAV orthophoto, focusing on the contact of the water-bank edge. Under the vegetation canopies, bank lines were delineated from the ground point cloud. This was possible due to using oblique imaging and varied UAV flight heights. In the areas with multiple channels, banks of the main and secondary channels were identified with a 4-m overlap. The planar water surface was calculated separately for all channels in a multichannel system and merged into one at the end of the water planar surface processing.

From the delineated bank lines, buffer polygons with a width of 5 cm were generated and used for the extraction of the bank point cloud. Each extracted bank point cloud underwent manual inspection, ensuring its classification solely as a ground point, free of noise and vegetation obstructions. After verification, this bank point cloud was refined using an average filter with a 10-cm diameter. Empty spaces,

notably hollows in sections with sparse point cloud densities, were linearly interpolated.

Perpendicular transects spaced 2 m apart were created along the channel centreline. Points of intersection between these transects and the bank lines were extracted, and smoothed elevation of the bank point cloud elevation values (based on averages) were assigned to these points within a 50-cm distance. These points of intersection were then moved to the transect endpoints situated 5 m away from the channel bank lines. Transect endpoints with bank elevation information were used for water surface interpolation via Delaunay triangulation. The resulting triangulated irregular network (TIN) surface was rasterised and refined using a focal statistic filter with a 1-m radius, smoothing any harsh triangulation edges.

Water surfaces were produced separately for main and secondary channels and were later merged into a single water surface. This consolidated raster water surface was exported to CloudCompare together with point cloud derived from the UAV survey. Channel depths were assessed using the Point-to-Mesh distance methodology. Negative values of water depth were used for filtering underwater points. Finally, we generated a new point cloud of underwater points with scalar field information about water surface elevation (*w_surf*) and the original elevation of underwater points (*sfm_z*). This point cloud entered the *pyBathySfM* software with camera position and orientation file to calculate corrected underwater point clouds. During the refraction correction phase, the filtering function was applied to consider only refraction angles that deviated less than 35° from the nadir, as cited by Woodget et al. (2019).

To validate the corrected point cloud derived from *pyBathySfM* software, validation points were measured during a concurrent field survey. For both field campaigns, depth measurement was taken by RTK, reaching position accuracy of 1–2 cm. Water depth was detected using a measuring tape mounted on a GNSS telescopic pole and manually assigned to the point attribute table. In total, 154 points were used for the 2015 and 200 for the 2022 bathymetry validation. To validate the corrected depth (refer to Table 4), the ME, the SDE, the MAE and the RMSE were calculated.

3.4 | Geomorphic analyses

3.4.1 | Long-term morphological evolution

Aerial images and orthophotos (1949, 1961, 1973, 1981, 1992, 2002, 2006, 2009, 2012, 2015 and 2018) were used from manual vectorisation of channel banks, gravel bars and islands in each time horizon. Channel width was measured as the average width of the active channel (AC) zone calculated as the sum of water area and

gravel bar within 100-m segments (Rusnák et al., 2016). The main threshold for bank delineation was the position of the vegetation edges on the floodplain. Expansion and contraction were detected by superposition of the consecutive channel active zone polygons (Ham & Church, 2012) using the Symmetrical Difference toolbox in ArcGIS. Expansion was defined as a movement of AC on the position of floodplain (erosion) and contraction as a transformation of AC to floodplain between two consecutive horizons. Furthermore, the river was longitudinally intersected by a channel segment with a spacing of 100 m using the Fluvial Corridor toolbox (Roux et al., 2015). The statistical significance between the medians of active channel width in the study years was analysed by a pairwise Wilcoxon test (nonparametric test for nonnormally distributed samples) with Bonferroni corrections between individual periods with a significance level ($\alpha = 0.05$). Moreover, a Shapiro–Wilk test was performed to calculate normality. Vectorisation error was estimated to 50 cm, based on orthorectification accuracy from aerial photo processing (see technical information in the Supporting Information section S2).

3.4.2 | Detection of incision based on analyses of historic floodplain channel surfaces (FCS)

Channel incision over an extended period was identified by using an innovative approach involving floodplain spatial memory extracted from LiDAR data. Historical vertical changes were detected for the period 1949–2020. This approach combines information from the floodplain age map (FAM) and detrended DEM (*dedDEM*). The FAM layer was created as a spatial union of all active channel polygons of each time horizon, and the method is described in detail in the paper by Greco et al. (2007). The final FAM layer includes spatial–temporal information about the river's channel position in different years that was extracted from the aerial photograph's origin (see Figure 5). If these older positions of the river are hanged above the present channel, it indicates channel incision. Detrended DEM identified heights of vertical surfaces above the river water surface at the time of imaging of LiDAR data. Here, water surface elevation from LiDAR is actual channel elevation, and *dedDEM* defines heights of older, abandoned fluvial geomorphic features extracted from the FAM layer (Figure 5) on the floodplain. These surfaces then have different heights above the present channel position (historical memory).

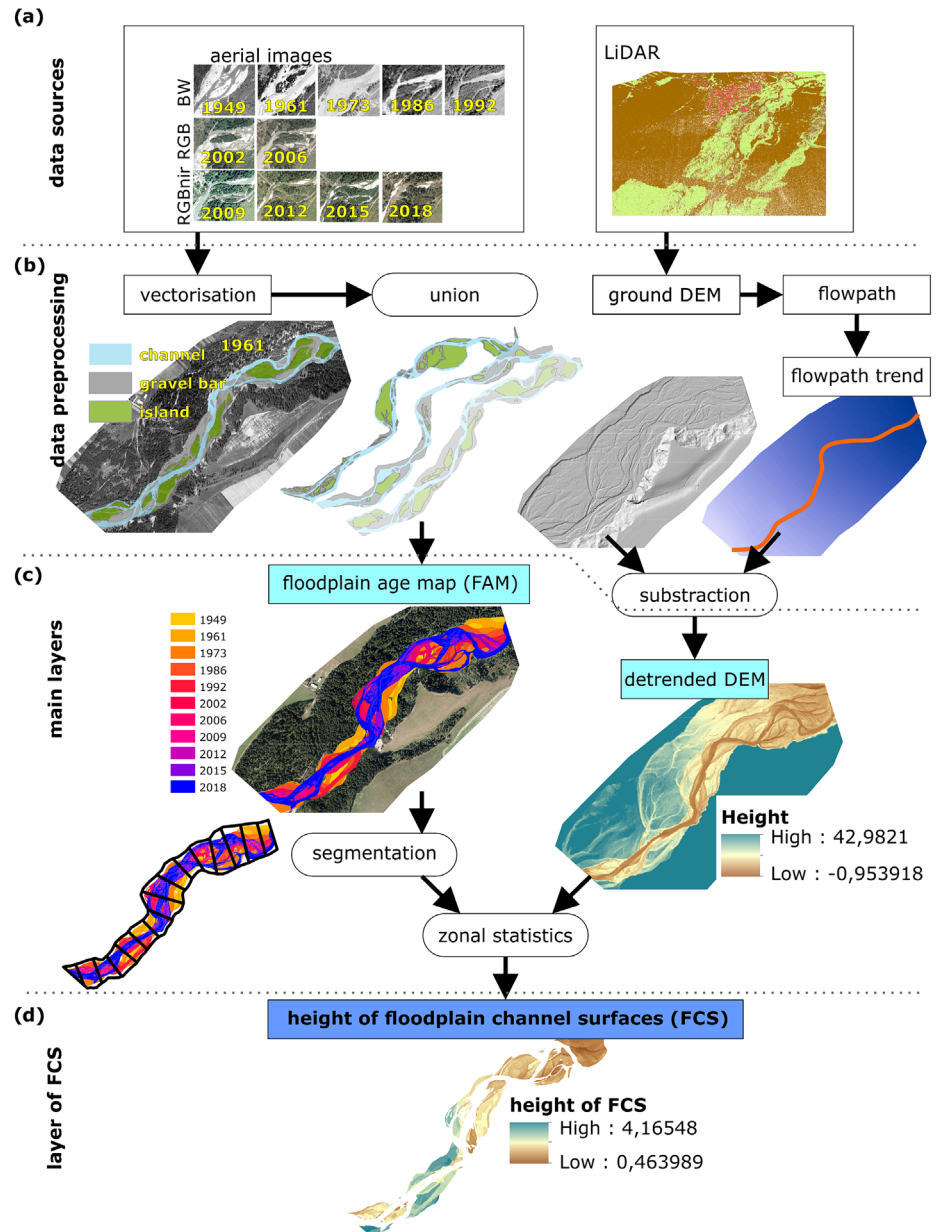
Finally, after a spatial combination of these two datasets, we obtain information about historical FCS, which are former channel positions dated by aerial images (from the FAM layer) and their heights above the channel are extracted from *dedDEM*. Differences between LiDAR data from 2020 and aerial images from 2018 were manually checked to fit channel edge differences, and we consider channel position in 2018 and LiDAR model 2020 as one and the same.

For statistical interpretation and longitudinal stationing, we used 100-m-long channel segments. The attribute table of the FCS contains average surface heights above the channel calculated by zonal statistics for all polygons created by intersection of 100-m segments and FAM. This table was exported from GIS as a DBF file and processed in RStudio software. The incision from 2011 was validated and interpreted by field channel cross-sections.

TABLE 4 Quantification of errors for deriving submerged topography using the multiview refraction correction method.

Year	<i>n</i>	Depth error			
		ME	SDE	MAE	RMSE
2015	154	−0.0164	0.1289	0.1018	0.1295
2022	200	−0.0045	0.1115	0.0861	0.1113

FIGURE 5 Workflow for identification height of floodplain channel surfaces (FCS) using two main data sources: aerial photographs and LiDAR point cloud (a); data preprocessing (b) and generation basic layers (c) of floodplain age map (FAM) and detrended DEM for calculation final layer of FCS by zonal statistics (d).



3.4.3 | Detection of incision volume based on analyses of FCS

The incision detected based on the FCS (see details in Figure 5) using a combination of LiDAR data and dated aerial images enables estimation of the eroded volume by incision from 1949.

The control (REF) section was used for the identification of the threshold for distinguishing between the natural height of the channel bank in reaches that are not impacted by incision and height that pointed to channel degradation. Incision volume calculation was performed only for channel sections where height of FCS is higher than the bank heights from 1949 in the REF section. This threshold was defined as a 75th percentile of FCS height dated to 1949 (oldest surfaces) for the REF section. The 75th percentile was selected for a more conservative estimate of natural bank height (as is mean or median) to reduce uncertainty.

The incision volume estimation was calculated by using the FCS approach (dedDEM, FAM layers) and a combination with the active channel zone area (Figure 6). Channel incisions are detected by

differencing heights of older channel positions above the current channel (height of FCS). For each segment and year, we identified the average height of FCS above the present channel and the channel's active area. In the cases where FCS height was missing in some years in a particular segment, these height values were automatically filled by interpolation function *na.approx* (zoo package) in RStudio to replace missing values between time horizons.

Furthermore, we identified differences in the height of FCS between two consecutive horizons in every segment. Negative differences are related to the processing errors and were transformed to value zero (segment without incision in the particular time period). These errors are related to complicated floodplain topography with varied elevation or processing errors (result of averaging for 100-m segments). The volume of incision for two consecutive time horizons and for every segment was calculated by multiplying the AC area of the younger horizon by height differences between FCS (one period). This calculation was applied only for segments where the value of the maximum incision (heights of FCS from 1949) was greater than 0.976 m. This value was calculated based on statistical

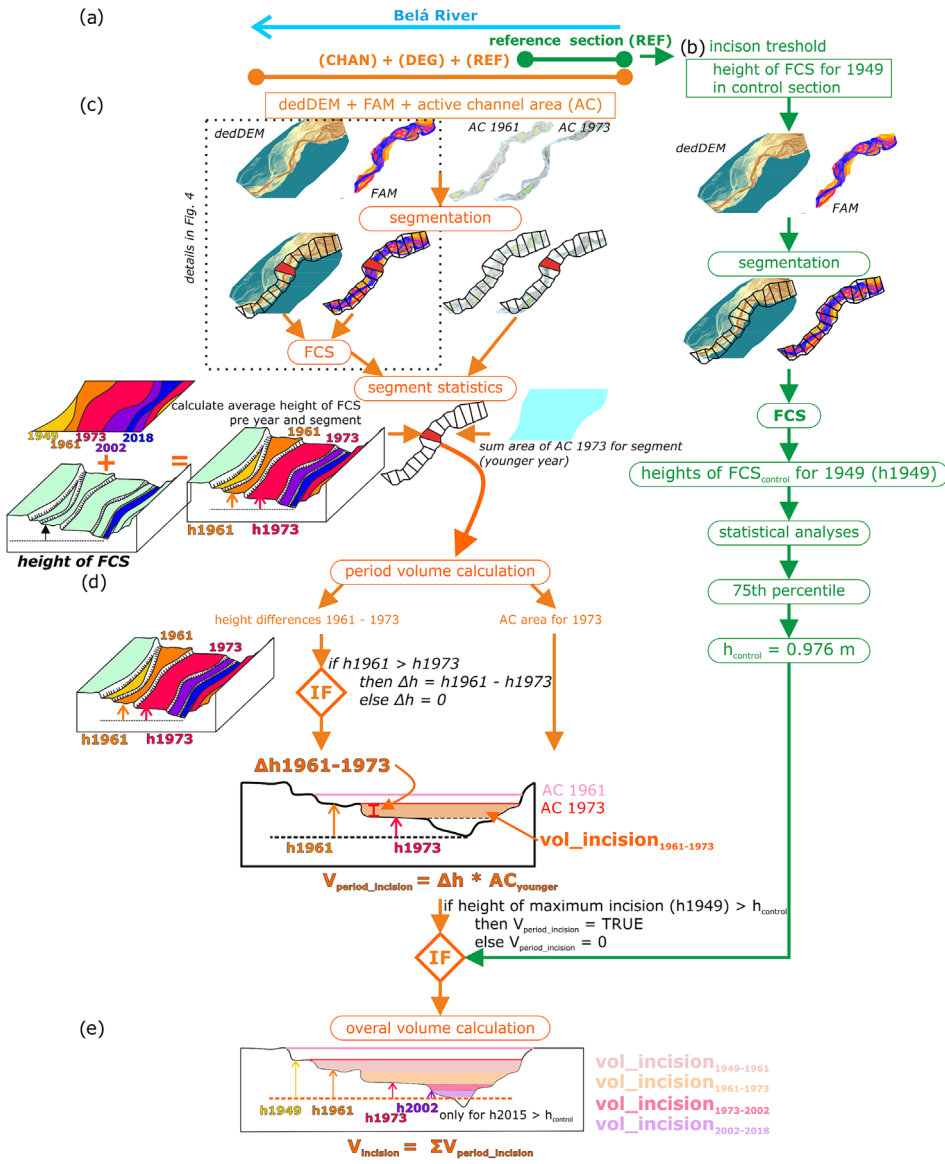


FIGURE 6 Process of calculation of incision volume for the whole river section and threshold calculation only for the control (REF) section of the Belá River (a). Only channel bed changes higher than the threshold of 75th percentile for heights of FCS from 1949 were used in the calculation (b). Eroded volume was estimated by using dedDEM, FAM layers and active channel area for each river 100-m segment (c). An example of eroded volume calculation for two-time horizons (1961 and 1973) by multiplying an active channel area 1973 (younger horizon) by differences of FCS heights in the given period 1961–1973 (d) and the process of overall volume calculation (e).

analyses as a 75th percentile of FCS height dated for the year 1949 in the control section (REF). Also, incision volume for the last period volume (2015–2018) was determined only for FCS heights higher than 0.976 m.

Finally, the overall volume was calculated by the addition of all period volumes for each river 100-m segment.

3.4.4 | Calculation of volumetric changes from UAV survey

Volumetric changes were detected by DEM of differences (DoD) and subtracting elevation values in the raster calculator. A combined elevation model for dry areas and bathymetry derived from the UAV survey was used for analyses. Pixel resolution of the final combined DEM was 10 cm. An elevation model of the submerged areas (wet) was generated from a corrected pyBathtSfM point cloud with the same spacing of 10 cm and clipped only to the extent of the water surface delineated from the orthophotos. Vegetation mask for both surveys was created from orthophotos, and all vertical changes outside the mask were excluded from the analyses.

For DoD, the change detection threshold was identified by evaluating the level of detection (LoD) to express an uncertainty value for the entire DoD (Brasington et al., 2003; Wheaton et al., 2009) expressed by the following equation:

$$\delta u = \sqrt{(\delta z_{\text{post}})^2 + (\delta z_{\text{pre}})^2}$$

where propagated uncertainty (δu) is calculated from the individual uncertainties (δz) for old (*pre*) and new (*post*) topographic surfaces. Vertical differences between UAV surveys were calculated in the Geomorphic Change Detection extension for ArcMap (available at <http://gcd.joewheaton.org/>; see Wheaton et al., 2013). In the DoD calculation, probabilistic thresholding was applied based on a confidence interval at a 95% level. SDE associated with wetted and dry channels was used as the error surface in DoD calculation with uniform error values for wet and dry surfaces (Table 5) due to the use of hybrid DEM constructed by different techniques. For the wet channel, we used depth error from validation of the bathymetric model (SDE 0.123 and 0.112 m, respectively), and dry channel error was associated with SDE of the checkpoint's errors in the z-direction (0.056 and

TABLE 5 Propagated uncertainties in Z dimension (m) calculated for DOD (δu_{DOD}) and propagated uncertainties at 95% confidence intervals ($\delta u_{DOD95\%}$) for different sources of δu .

Source of uncertainties	δu_{DOD} (m)	$\delta u_{DOD95\%}$ (m)
Dry-dry	0.0575	0.0946
Dry-wet	0.1108	0.1823
Wet-dry	0.1324	0.2177
Wet-wet	0.1628	0.2678

0.0135 m, respectively). Therefore, cells with probability values less than critical threshold error, based on a 95% confidence interval, were considered uncertain and not used in the computation.

3.4.5 | Incision detection from UAV survey

The assessment of incision and maximum vertical channel bed changes between UAV flights in 2015 and 2022 was performed by comparing the minimal underwater elevation in the transects perpendicular to the channel centreline with 10-m spacing. The transects were densified by vertices with a distance of 20 cm (double of DEM resolution), and for every vertex, the elevation from both bathymetric DEMs was extracted. Differences between minimal elevations greater than 0.268 m (max $\delta u_{95\%}$ from Table 5) in every individual transect were marked as channel incisions in a given transect and pointed to vertical bed changes detected from the UAV survey.

4 | RESULTS

4.1 | Long-term morphological evolution

The Belá River has gradually changed from a braided multichannel pattern to a wandering, single-channel gravel-bed river. Active channel width has decreased throughout all studied sections from approximately 80 to 31 m (Figure 7a). The width of the channelised river section (CHAN) underwent a statistically significant decrease from 1949 to 1961 (p value = 0.037) and also significantly differed for all periods between 1973 and 2006. In 2018, the active width was 32.1 m. In the degraded (DEG) and natural (REF) sections, active channel width decreased significantly after 1973 with p value of 0.0002 (DEG) and 0.0110 (REF). In the DEG section, the width only significantly differed during the period 1986–2002. By contrast, the REF section showed greater variability in its active channel width after declining from 1973.

The channel bar (Figure 7b) area decreased from 3741 m² per 100 m of channel length for the CHAN section to 1813 m²/100 m in 2018, with a minimum between 2002 and 2012 (917 and 770 m²/100 m, respectively). The DEG and REF sections exhibited similar patterns of gravel bar evolution, with a large decrease after 1973, from 5522 m² per 100 m (4499 m²/100 m for REF) to 2963 m²/100 m (3398) in 1986, as well as considerable variation after 1986 related to increased flood activity (Kidová et al., 2016).

The average lateral channel migration (expansion) rate (per year and 100-m-long segments) was in the CHAN section 88.9 m², 166.9 m² in DEG and 210.9 m² in REF (Figure 7c). The contraction rate during the whole study period 1949–2018 was 123.8 m² for CHAN, 214.4 m² (DEG) and 257.9 m² (REF section). The average ratio for the whole study period between expansion and contraction was positive (prevailing contraction), with values of 34.99 m² (CHAN), 47.46 m² (DEG) and 47.68 m² (REF) per year and 100-m segments. All channel sections expressed the same temporal variability in lateral activity, differing only in the intensity of these processes.

4.2 | Incision detected from historical FCS

Channel bed incision was detected in the CHAN and DEG section of the Belá River. The oldest channels after river incision are now hanged on the floodplain as vertically dissected surfaces. Historical FCS analyses point to the presence of channel incision in the CHAN and DEG sections (Figure 8). Here, the average height of all dated FCS is 0.94 m in the CHAN section and 1.59 m in the DEG section. While in the control REF section, the average height of all FCS is 0.47 m above the actual channel position and corresponds to the height of the natural bank (Figure 8a). The temporal evolution of the FCS in a given year in the CHAN section shows its decrease in a median height from 1.64 (1949) to 0.62 m for surfaces dating to 2015. The highest vertical differences were observed in the DEG section, with a median height of 2.73 m for FCS in 1949 and 1.14 m for FCS in 2015. In the REF section, median heights varied around 0.4–0.6 m for all dating FCS. The height of the FCS dated only to 1949 pointed to the overall incision in the period 1949–2020.

The longitudinal evolution of all dated FCS heights above the channel (Figure 8b) indicates an intensive channel incision in the middle part of the studied reach between km 3 and 7. The results from the downstream part of the CHAN sections (km 0–1.5) do not point to the channel incision. In this river section, an incision occurred around kilometre 1.5 and especially from kilometre 2.8. The DEG section's median height of floodplain surfaces ranges from 0.87 to 3.04 m, but the highest values were attained in river kilometre 5.5 with the maximal height of FCS above 5 m. From this river segment, the height of FCS continuously decreased to the REF section.

Plotting FCS only for 1949 (Figure 8c) portrays the longitudinal evolution of channel incision in the period 1949–2020. In the CHAN section, incision started from river km 1.5 to 3.2 with a maximum on the border between CHAN and DEG section at value 4.05 m (km 4.8). In the DEG section, the height of the floodplain surfaces declines from 5.05 m (river km 5.5) to 3.4 m (river km 6.0) with gradual decreases to river km 7.0, where the heights of the floodplain surfaces are in the range of the bank height.

Historical FCS from 1949 reflect a median incision rate of 0.025 m/year. This value was calculated from the median height of 2.73 m of the 1949 FCS in the DEG section. In this calculation, natural bank height threshold (0.976 m) was applied, which was subtracted from the FCS₁₉₄₉ median height. The maximum incision rate calculated from the maximum values of the 1949 FCS achieved 0.057 m/year.

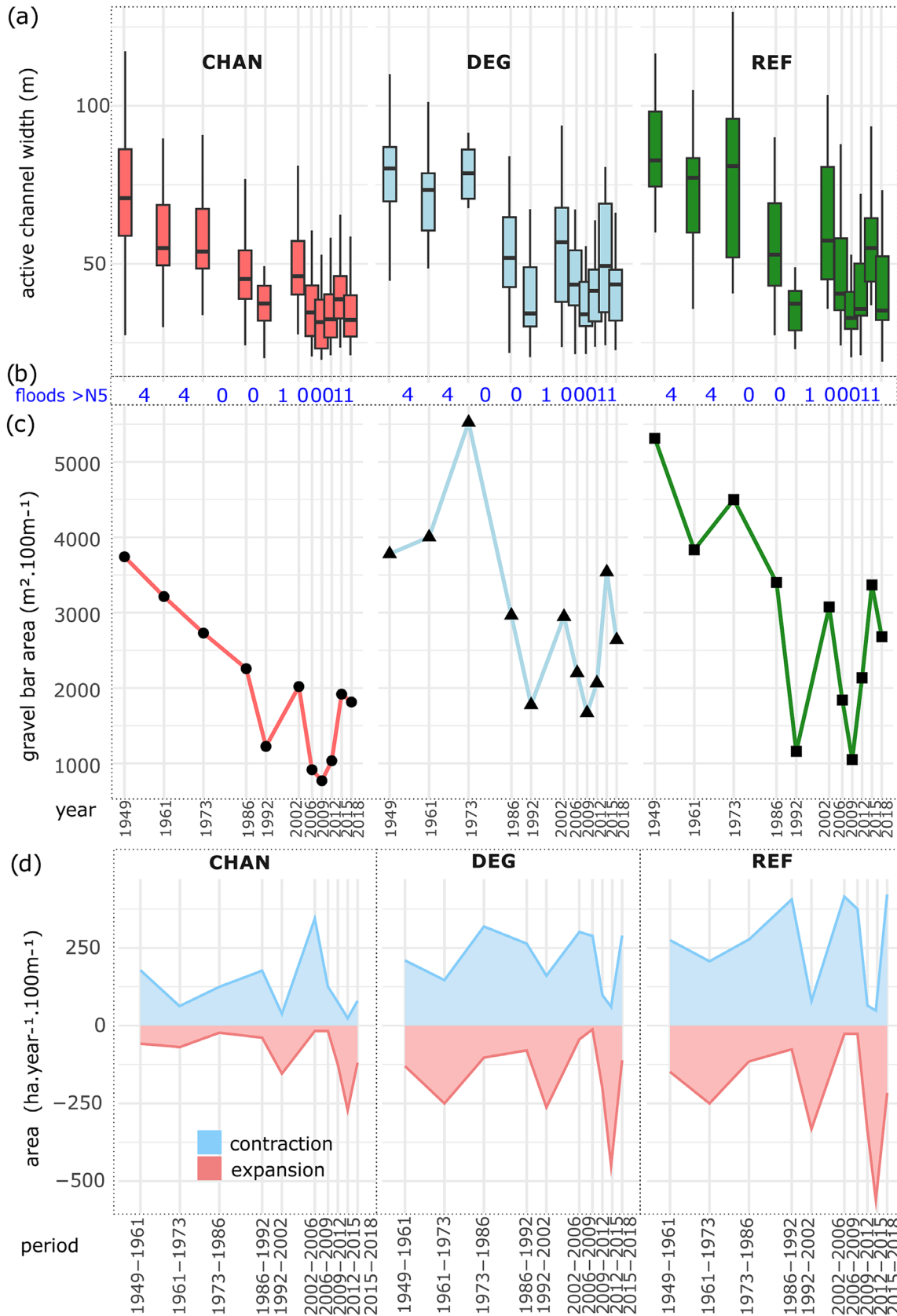
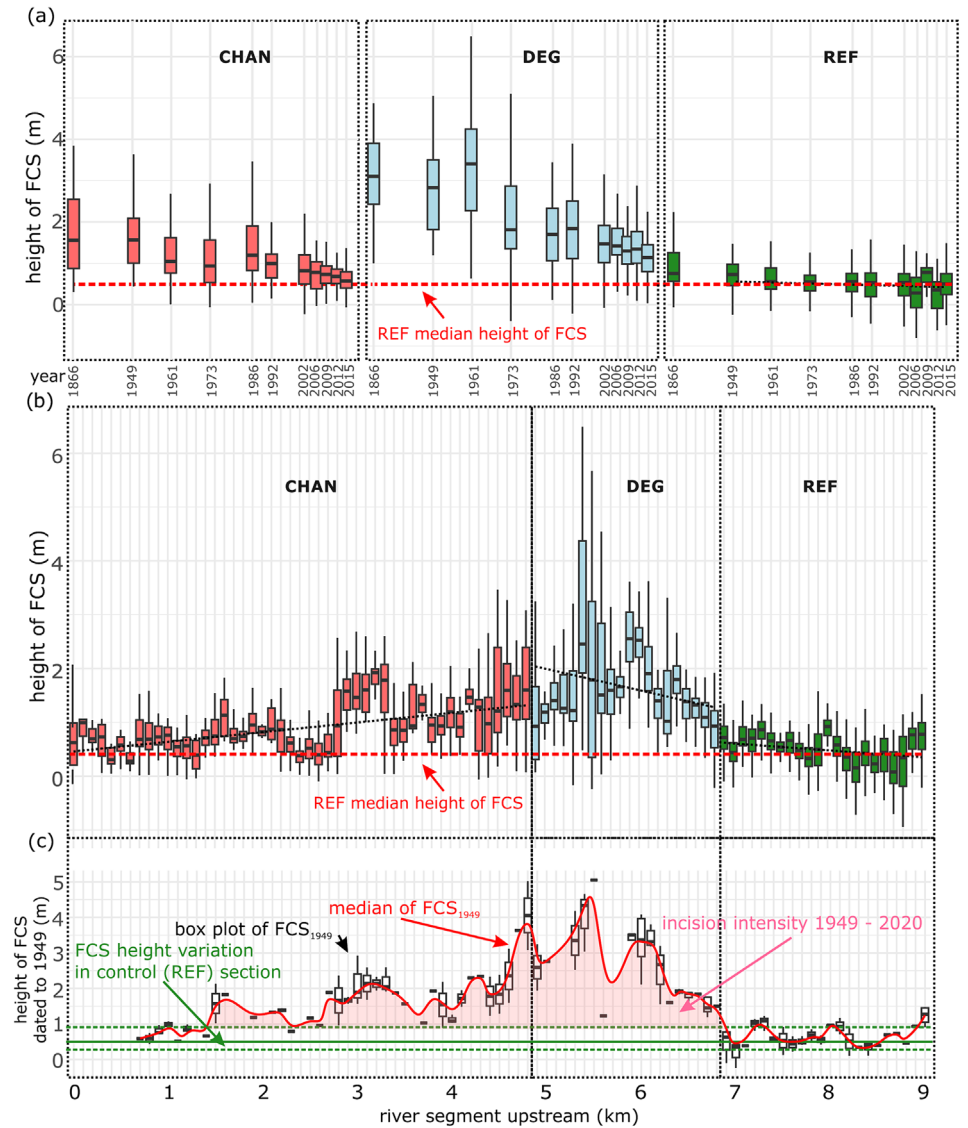


FIGURE 7 Temporal evolution of the active channel width (a); numbers of flood events with floods >5 years return period (b); gravel bar area per 100 m of river segments (c); and area of expansion and contraction (d) calculated per year and 100 m of river segments between 1949 and 2018 for the Belá River in selected river sections (CHAN, DEG, REF).

FIGURE 8 Temporal evolution of the heights of floodplain channel surfaces (FCS) in period from 1866 to 2015 for CHAN, DEG and REF sections (years 1866 and 1949 not in scale) of the Belá River (a); longitudinal evolution of FCS heights for CHAN, DEG and REF section (b). The black dotted line represents the linear trend for each river section, and the red line is the median height of FCS in the control REF section. Longitudinal evolution of FCS height dated to 1949 (black and white box plot), with the median course of FCS₁₉₄₉ heights (red line), FCS height variation calculated from control (REF) section calculated (median for solid green line and dotted line for variation) and incision intensity between 1949 and 2020 calculated as differences between FCS heights in 1949 and control section (red area).



4.3 | Incision volume estimation based on analyses of FCS

Overall, 589 704 m³ of sediment was eroded by incision and channel bed lowering based on the analyses of FCS height changes. The highest amount of 321 701 m³ was eroded in the DEG section, 253 602 m³ in the CHAN section and 14 401 m³ in the REF control section (Figure 9a). The temporal evolution of incised volume (Figure 9b) pointed to the decrease of eroded volume in the CHAN section from the period 1992–2002 and negligible values in the REF section. The intensity of this process (volume per segment) was the highest in the DEG section, with acceleration in the periods 1961–1973, 1992–2002 and 2012–2015. Longitudinal evolution of eroded incision volumes (Figure 9a) copies median of FCS height from Figure 8c.

4.4 | Channel cross-section changes over the last decade

Channel bed elevation changes were validated in the past 10 years based on the cross-sectional profiles (Figure 10). In the CHAN, the cross-section did not record vertical changes in the channel bed. During the last 10 years bed elevation in all profiles in the CHAN

section ranges up to 1 m, and sediment deposition with water flow shift within channel boundary is tracked. Locally, sediment deposition and channel bed raising are recorded (as in profile A or B). Measurement in the DEG section pointed to the maximal channel lowering of 2.5 m and abrupt channel narrowing from 35 m wide channel to 10 m incised one (changes represent profile C in Figure 10 and photographs in Figure 11). The rate of vertical erosion reached 25 cm per year at profile C (comparison with other approaches in Table 6). During the period 2011–2019, the former gravel-bed channel transformed into an incised claystone bedrock. The last period (2019–2021) is characterised by canyon widening and gravel deposition in the channel bottom, reducing the channel depth. Profile D (REF section) represents a natural river section without incision and prevailing active channel mobility during the study period. Channel shift is measured during every survey, and minimal channel depth fluctuates up to 1.5 m but without evident temporary trend.

4.5 | Volumetric changes and incision in the DEG section from UAV survey

Detailed analyses of topographic and volumetric changes in the DEG section (Figure 12a) by the photogrammetrically derived UAV

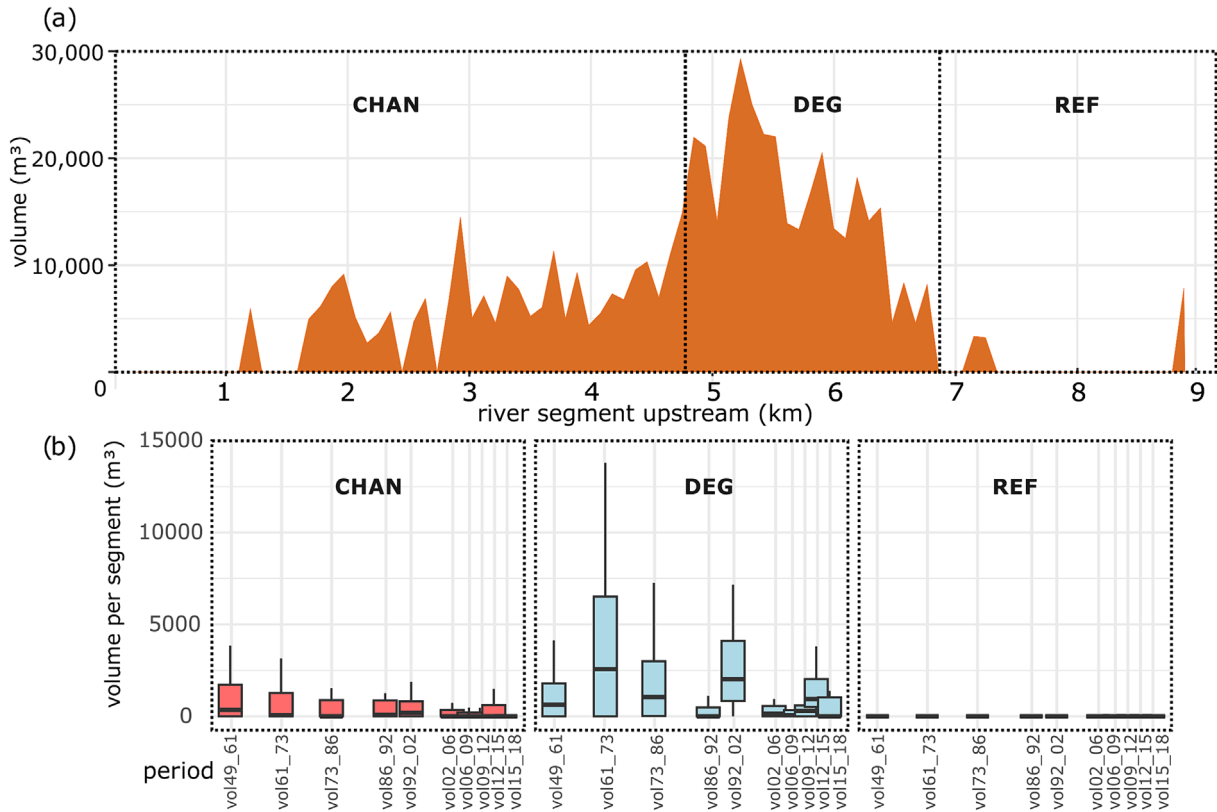


FIGURE 9 Longitudinal behaviour of eroded volume (a) and temporal evolution of eroded volume by channel incision for 100 m long channel segments in CHAN, DEG and REF section (b).

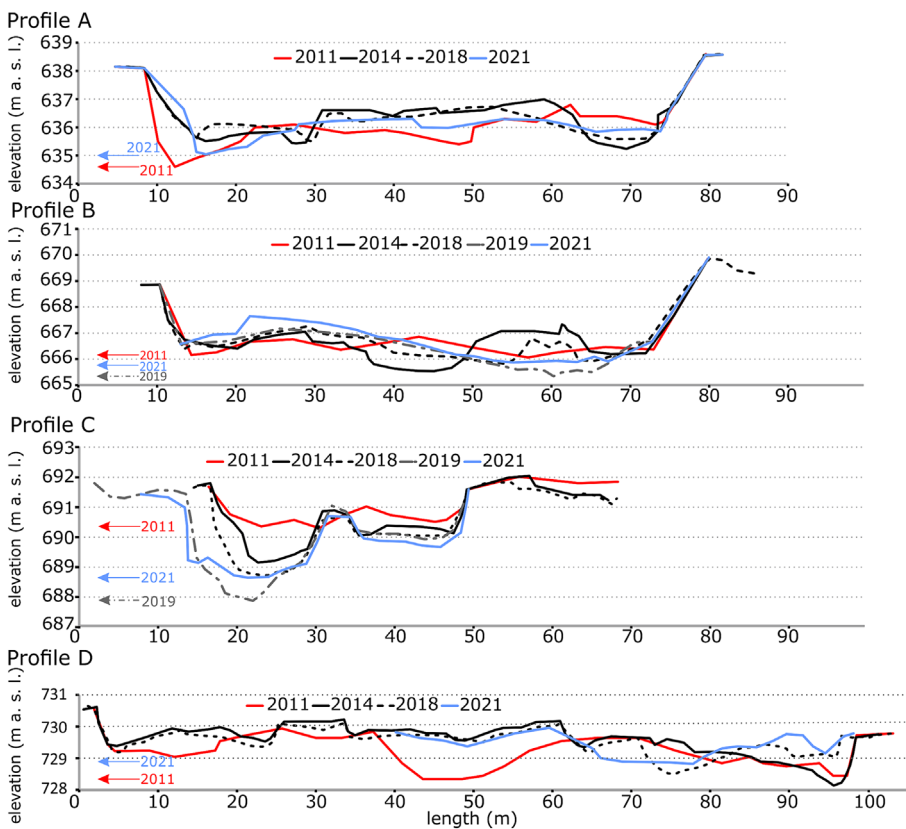


FIGURE 10 Channel cross profile for the CHAN (profiles A and B), DEG (profile C) and REF sections (profile D) between 2011 and 2021. For the location of the profile, see Figure 1. The arrows on the left side indicate the maximum depth of the channel during different measurements.

elevation bathymetric models point to ongoing incision and upstream migration of headcut front. Upstream migration was 85 m/year in the period 2011 (position detected during fieldwork) and 2015 (UAV

survey), where the headcut was moved in the former main channel by 340 m upstream (zone B in Figure 12b). During the period 2015–2022, headcut front moved by 567 m, what was reflected in high

FIGURE 11 Transformation of the gravel-bed channel in 2011 (a) to the incised channel system on claystone bedrock in 2018 (profile C in Figure 7) with vertical differentiation of up to 2.5 m between water level elevations for the main and secondary channels (b).

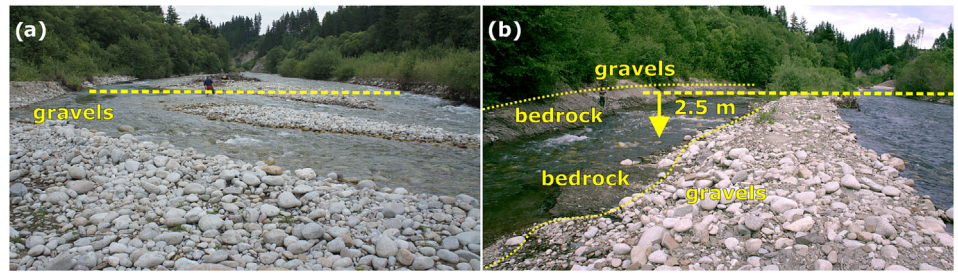


TABLE 6 Incision of the Belá River and intensity of incision detected by different approaches for CHAN, DEG and REF section.

River section	Approach applied						Cross-section (2011–2021)		UAV bathymetry (2015–2022)		
	FCS ^a (1949–2020)			FCS1949 ^b max.			Profile	[m]	Intensity (cm/year)	(m)	Intensity (cm/year)
	FCS (m)	FCSbank ^c (m)	Intensity ^d (cm/year)	FCS (m)	FCSbank ^c (m)	Intensity ^d (cm/year)					
CHAN	2.73	1.754	2.47	4.05	3.074	4.33	B	0.98	9.8	x	x
DEG	1.64	0.664	0.94	5.05	4.074	5.74	C	2.45	24.5	1.39	19.86
REF	0.74	0	0.00	2.06	1.084	1.53	D	-0.48 ^e	-4.8 ^e	x	x

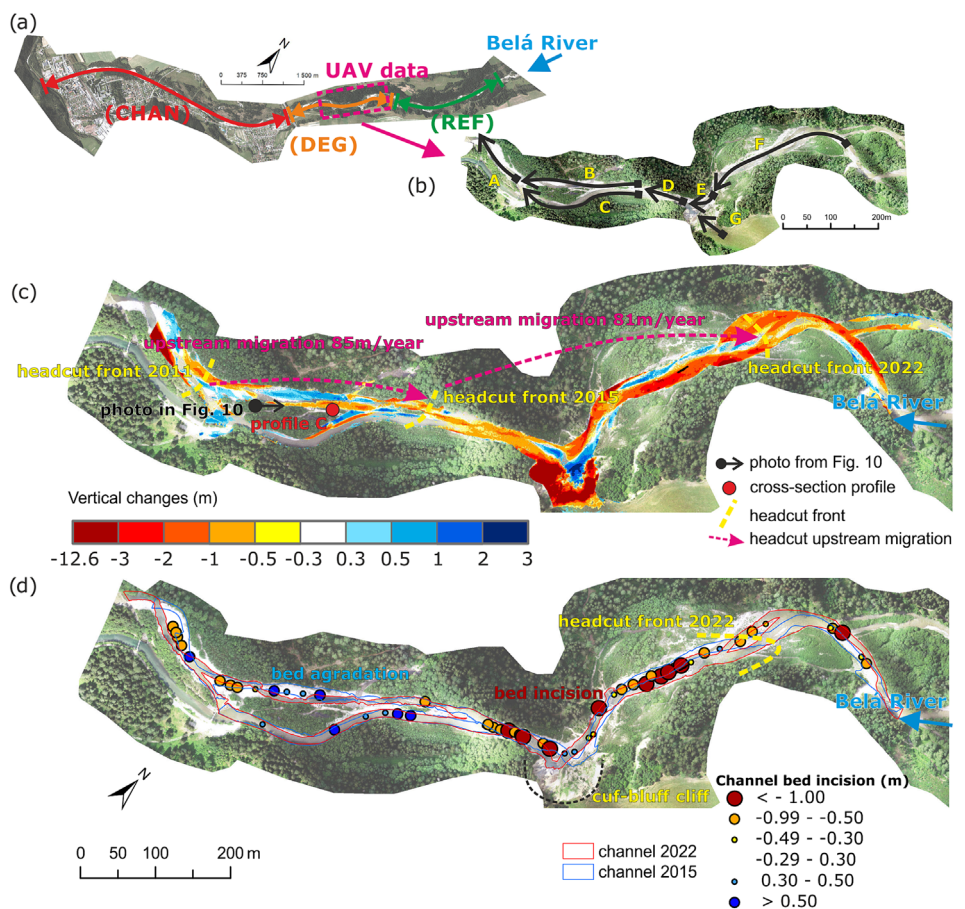
^aMethod using the calculation of floodplain channel surfaces (FCS) height above the present channel.

^bHeight of FCS dated to 1949.

^cHeight of FCS lowered by natural bank height of 0.976 m.

^dIntensity calculated from FCS with natural bank height threshold; ^e negative values pointed to the process of aggradation.

FIGURE 12 Detailed analyses of channel bed incision in the DEG section of the Belá River (a) by UAV surveys in 2015 and 2022 in different channel zones marked by letters A–G (b) with the classification of the channel to 7 basic morphological units (A: channel parallel with hydro powerplant; B: former main channel; C: main channel (supply channel and maintained); D: single channel under cut-bluff cliff; E: meander undercutting cut-bluff cliff; F: single channel above cut-bluff cliff; G: cut-bluff). Morphological changes and vertical elevation changes in the river channel (c); and channel bed incision rate between 2015 and 2022 with channel position and orthophoto from UAV survey in 2022 (d).



DoD vertical changes (Figure 12c) and bed incision (Figure 12d) in this river section (zone D and F). The highest amount of eroded material is related to propagation of headcut migration. Overall, DoD pointed to the mobilisation of 31 876 m³, of which 27 318 m³ was eroded, and 4559 m³ was deposited (Table 7). The net amount of sediment eroded in this river section during the period 2015–2022 was –22 759 m³ with the highest ED index (rate between eroded and deposited material) in the zones D and F with headcut propagation. The DoD of the downstream part (zone A, Figure 12b), characterised by a particularly high erosion-deposition (ED) index value, indicated the combined effect of channel bed incision and the lateral erosion of the incised bank with a height of 3 m. The incised channel in zone B has been stabilised by lateral erosion and the widening of the incised channel, with gravel deposition on the channel bottom. The main flow channel (zone C), which has been maintained via human interventions to ensure water supply to the hydropower plant, has a balanced ratio between deposition and erosion. Volumetric changes there are strictly related to maintenance activities. Extreme incision resulting from headcut front migration has occurred in the middle and upper sections of the UAV survey reach, where DoD pointed to bed lowering of up to 1.39 m. The erosion-deposition ratio proved to be highest in zones D (–92.2) and F (–12.1). Here, sediment erosion is located exclusively in the channel bed and can be interpreted as a propagation of back erosion from downstream reaches. Gravel-grained sediment transport is supplemented by fine sediment input from undercutting cut-bluff cliffs (Rusnák et al., 2020).

5 | DISCUSSION

5.1 | Channel incision, embankment and mining matters

Historical aerial images confirm the overall transformation of the study river system, characterised by a channel narrowing and gravel bar shrinking. The BACI approach enables identified mutual cause-effect relationships of different driver's impacts by distinguishing temporal and spatial scales. Temporal scale is related to the aerial images enabling the date of the effect (*Pre* and *Post*) and spatial localisation of

reaches with direct propagation of impacts. Control sections located upstream from impacted reach are affected by channel transformation but without propagation of channel bed lowering. This pointed to the catchment scale impact on channel narrowing and local downstream drivers for channel incision.

Declines in active channel width and gravel bar area in all studied river sections (CHAN, DEG and REF) started in 1949 and are connected with catchment afforestation after the establishment of the national park (Kidová et al., 2016). This finding is consistent with an analysis of the 1866 historical cadastre map when the channel width is comparable with the width of the channel in 1949 (72 m in 1866 to 77.7 m in 1949). Moreover, the width of the channel is linked with 10-year return period floods that caused channel widening and increase of bar area in the period 1992–2002. The combination of smaller floods (<5 years) and deforestation in the upper catchment after 2002 continued to increase variability in active channel width, the gravel bar area and higher dynamics in expansion/contraction processes (Liébault & Piégay, 2002; Scorpio et al., 2018; Scorpio & Piégay, 2021; Ziliani & Surian, 2012). In 2004, an exceptional wind-storm caused 126 km² of forest damage in Tatras National Park between 700 and 1350 m a.s.l. (Falt'an et al., 2020, 2021). The upper catchment of the Belá River was only partially affected by forest damage, but this event triggered a serious (the largest ever recorded in Slovakia) bark beetle outbreak in the upper catchment area, which spread from the damaged forest (Kunca, 2013; Nikolov et al., 2014). This led to a decrease in forest cover (Figure 13) and higher channel dynamics in this period, with an increase in channel width, gravel bar area and lateral activity.

Incision evidence only in the downstream part below the control section (in the DEG and CHAN section) pointed to the local drivers affecting bed lowering. The maximum incision rate intensity from the FCS approach for Belá River was estimated to 0.057 m/year, which is comparable with other Alpine or Carpathian rivers (Škarpich et al., 2013), with an average incision rate ranging from 0.0115 m/year to 0.163 m/year. Moreover, the FCS heights dated from the old cadastre map in 1866 are identical to those in 1949 (Figure 8). This indicates the absence of significant vertical changes before 1949 and dates the start of channel incision in the CHAN section to 1949 and in the DEG section after 1961. This allows us to relate this bed

TABLE 7 Volumetric changes in different zones of the Belá River channel with net volume and ED index (rate between eroded and deposited material) between UAV surveys in 2015 and 2022.

Zone	Description	Eroded		Deposited		Net	ED	Bed changes (m)	Process ^c
		Vol. (m ³)	Error (±)	Vol. (m ³)	Error (±)				
A	Channel parallel with hydro powerplant	–3090	117	+398	94	–2692	–7.8	–0.814 ^a	LA, I
B	Former main channel	–2471	366	+1012	239	–1458	–2.4	–0.059	LA, GD
C	Main channel (supply channel and maintained)	–772	98	+957	175	+185	+0.8	0.1725	BAL
D	Single channel under cut-bluff cliff	–1365	288	+15	3	–1350	–92.2	–0.644 ^a	I
E	Meander undercutting cut-bluff cliff	–4214	227	+906	115	–3308	–4.7	–0.1945	LA, GB
F	Single channel above cut-bluff cliff	–15406	1229	+1270	252	–14 136	–12.1	–0.582 ^{a,b}	LA, I, GB
G	Cut-bluff sediment input	Input: 3368 m ³ /year (Rusnák et al., 2020)							

^aHigher than minLOD .

^bDownstream half of the F zone reach –0.882 m with maximum –1.282 m.

^cProcess: lateral erosion (LA), incision (I), gravel deposition (GD), balanced reach (BAL).

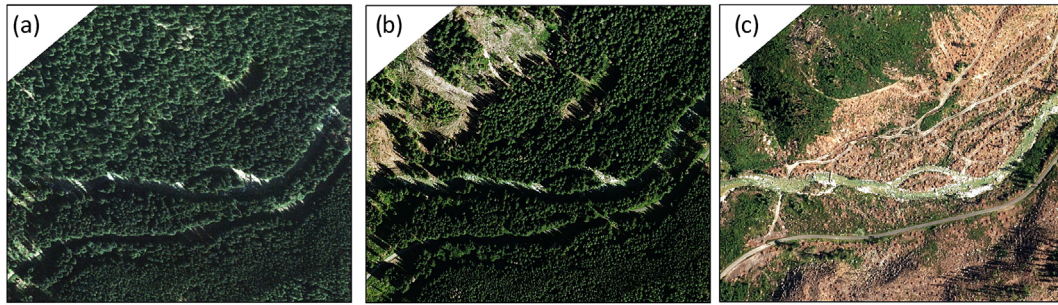


FIGURE 13 The upper catchment of the Belá River after the windstorm in 2006 (a) and the continuous increase in the bark beetle outbreak's impact on forest cover in (b) 2009 and (c) 2015.

lowering to active human intervention in the downstream section of the river channel, specifically with the commencement of channelisation works, embankment construction and gravel mining. These human interventions are considered the most important local drivers affecting channel bed lowering (Dufour et al., 2015; Hajdukiewicz et al., 2017; Korpak, 2007; Marston et al., 2003; Rinaldi et al., 2005; Surian & Rinaldi, 2003).

Incision volume estimated based on analyses of FCS pointed to the erosion of 575 303 m³ by incision in the DEG and CHAN sections. Technical documentation states the extraction of 140 000 m³ between 1950 and 2000 in the CHAN section during river regulation works. This amount is underestimated but still covers only 24% of sediment eroded in the CHAN and DEG sections, or 44% eroded only in the CHAN section.

Temporal evolution of eroded volumes pointed to higher dynamics in the DEG than in the CHAN section (Figure 9b), where eroded volumes increased in the period 1961–1973, 1992–2002 and 2012–2015. All these periods are linked with flood events and channel widening. This points to the direct connection of the channel lateral expansion and incision, which we cannot remove from the overall volume evaluation. At the same time, processes leading to bank erosion with lateral activity (expansion) and aggradation can occur during the period between imaging.

To summarise, channel incision was triggered by the channelisation process in the CHAN section supported by gravel extraction (Figure 14). Later onset of the channel incision in the DEG section pointed to the upstream propagation of the channel bed erosion after local channel base lowering from CHAN section. Moreover, the confluence has been affected by the lowering of the Váh River's streambed, which previously initiated backward erosion from the junction of the rivers until this was stopped by the construction of the stony-grade structure. Backward erosion and knickpoint migration (Kondolf, 1997) in the DEG section started after channelisation work and are spatially connected with the channel embankment.

5.2 | Ongoing process: incision propagation from UAV

UAV surveys and channel cross-sections pointed to gradual propagation of the channel incision in the last decade, when bed lowering reached 0.0223 m/year in the period 2011–2022, identified from cross-sections and upstream headcut migration of 82 m/year. Nowadays, direct artificial impact by the maintenance of the water

supply channel to the hydropower plant and gravel mining is still occurring in the DEG section. This accelerates the process of degradation and headcut upstream migration. Flow concentration to narrow and incised channel increases stream power (Wyźga, 1993; Wyźga, Zawiejska, & Radecki-Pawlik, 2016) and backward erosion by knickpoint retreat. Channel narrowing and bed erosion have led to outwash gravel infilling of the channel bed, and the incision has continued to bedrock layers, especially in less resistant rock. Examples from the Czech Republic and Spain provide evidence of extraordinary in-channel bedrock incision up to 8 m related to dam construction (Škarpich et al., 2013) or the combined effect of channelisation and gravel mining (Ferrer-Boix et al., 2023).

The process of incision in the DEG section is directly related to the backward erosion with the highest incision rate in the headcut front. The degraded river channel downstream this knickpoint adheres to Simon and Hupp (1987) general model of channel evolution, whereby the degradation phase is followed by a widening and aggradation phase until a new quasi-equilibrium is reached. The DoD changes in the DEG section also confirm gravel aggradation on the channel bed (zone B in Figure 12b).

The DoD from the UAV survey pointed out that in this section was eroded by an incision of $-22\,759\text{ m}^3$ of gravels, with a total mass of $\sim 45\,700$ tons calculated from a bulk density of 2.69 g cm^{-3} for granitoid and metamorphic rocks of the Tatricum unit (Šamajová & Hók, 2018) and a porosity of 0.25 (Martin & Church, 1995; Surian & Cisotto, 2007). Furthermore, during this period (2015–2022), another 60 583 tons of fine-grained claystone sediment entered the channel system from the undercut cliff in the middle of the DEG section (Rusnák et al., 2020). This eroded amount, approximately $23\,000\text{ m}^3$ from a 1.6 km long reach of the Belá River, is comparable with other Flysch Carpathians river Morávka, where the volume of $39\,000\text{ m}^3$ (850m long reach) in the period 2010–2014 was eroded as the effect of hungry water below the dam (Škarpich et al., 2020). In Poland, Hajdukiewicz et al. (2019) calculated an amount of $11\,780\text{ m}^3$ of sediments eroded from the 3 km long reach of the Czarny Dunajec River from 1964 to 2009.

The upstream amount of sediment entering the whole system is unknown. Although channel morphology parameters such as channel width and gravel bar area have shown a decreasing trend, the Belá River preserves lateral dynamics by contraction and expansion of the channel (Figure 7). Moreover, the general morphology of the channel is sensitive to overall catchment changes (deforestation) and to changes in flood intensity (Kidová et al., 2016), which can affect sediment transport (Downs et al., 2013). The result was an increase in

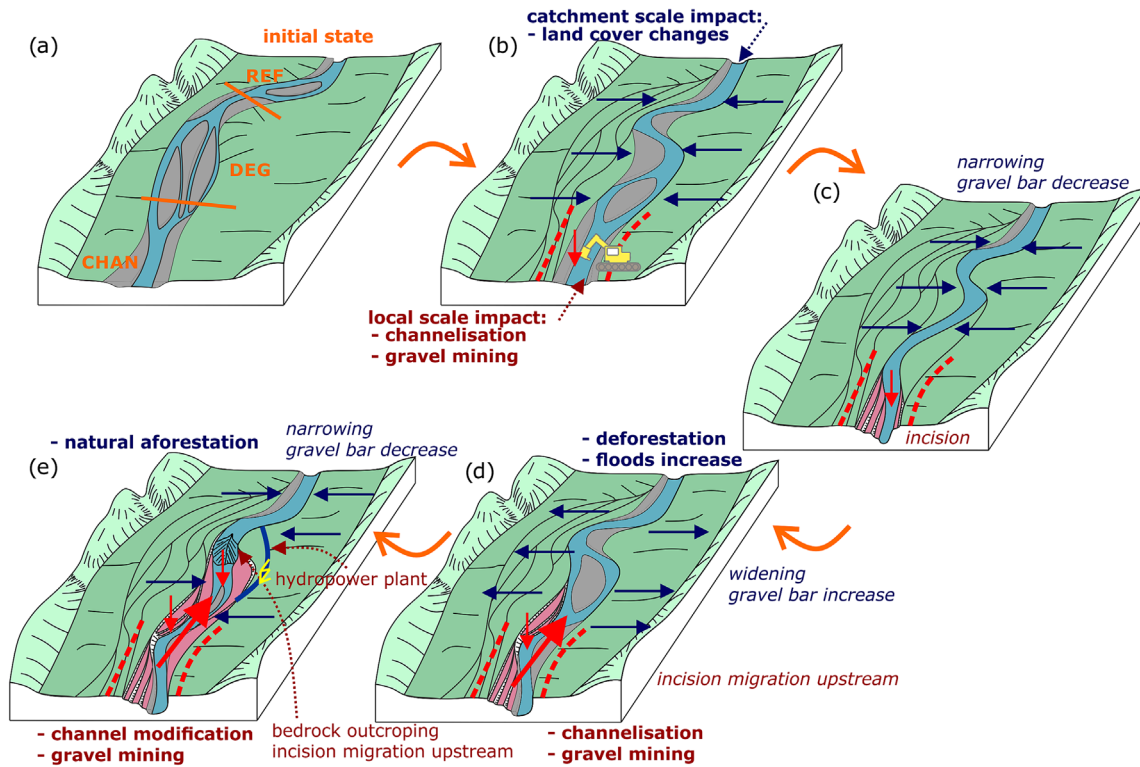


FIGURE 14 Conceptual model of the channel evolution from the initial state of a wide and braided channel (a); and channel affected by upstream impacts (catchment scale) and local human interventions (b). These impacts led to channel narrowing and downstream incision (c). Changes in the forest cover and floods led to channel widening, increasing the gravel bar area and continued upstream incision migration (d). Continuing the catchment natural afforestation, a decrease in flood activity, active negative human interventions, and gravel mining transform the channel by bedrock incision and headcut migration (e).

lateral dynamics in both control (REF) and incised (DEG) river sections during the past 15 years. This confirms that natural sediment transport is still sufficient in the control section and proves the continuum of sediment to the downstream part of the CHAN section. Sediment continuity and lateral channel dynamics are necessary to preserve gravel-bed rivers in mountainous catchments or for the revitalisation process (Brousse et al., 2021).

5.3 | Benefits of remote sensing information: dating and budgeting

The application of historical aerial images with LiDAR topography is a valuable source for long-term channel incision monitoring and assessment. Moreover, this approach enables the extraction of both (spatial and temporal) dimensions of channel incision. Aerial images are used for dating (time scale) and framing channel changes (space scale) in longitudinal and lateral directions. Vertical information added from LiDAR with historical channel positions can create the three-dimensional spatiotemporal evolution of a channel incision (Lallias-Tacon et al., 2017). Furthermore, in the areas without historical cross-sections or longitudinal profiles enable automatic detection of incision in hot-spot areas, even their local presence. Field photographs and bridge undercutting data (Ferrer-Boix et al., 2023; Galay, 1983; Kondolf & Swanson, 1993) are essential for validation but provide discontinuous datasets. The benefits of a combination of LiDAR and aerial images lying in the fully continuous information for interpretation of channel incision temporally (Figure 8a) and

longitudinally (Figure 8c). Spatial approach with the height of FCS in different years, combined with active channel area allowed detection of eroded volume for the whole or particular period or river section. For valid interpretation, well-distributed FCS in longitudinal and temporal dimensions are required, whereas older channel surfaces are often destroyed by newly formed ones. Anyway, also partially reconstructed FCS can be used for the interpretation of vertical position and channel incision, as is field surveying by GNSS (Calle et al., 2017) or cross-section profiles detection of hanging surfaces (Liébault & Piégay, 2002). The automatic process ensures to capture of all surfaces which can be unnoticed in the field measurement that are overgrown with vegetation or inaccessible.

Historical incision rates are confirmed by UAV channel bathymetry survey with an accuracy of DoD up to 26 cm. Hajdukiewicz et al. (2019) applied historical aerial images by traditional photogrammetry DEM generation for the detection of incision in Czarny Dunajec River between 1964 and 2009 with processing error of 30–40 cm and demonstrated a progressive upstream shift of incision. A combination of the historical aerial images and SfM processing used Llana et al. (2020) for the identification of channel incisions by extracting continuous channel longitudinal profiles for 1957 and 2015. In both cases, photogrammetrically processed data enable direct bed-lowering measurement. The indirect approach that uses morphological evolution of floodplain has also been applied to analyse the elevation differences between the active channel and the abandoned channel in the period 1949–1970 using a detailed topographic survey for small pre-Alpine tributaries with incision of 1.31 ± 0.6 m (Liébault & Piégay, 2002).

Floodplain elevation (FCS) analyses (Figure 8) have the limitation that natural bank heights must be incorporated into incision calculation. For the Belá River, the control REF section was used for identification of natural bank heights. These vertical changes of FCS that are lower than bank height cannot be interpreted as an incision. Moreover, without historical floodplain topography data and the initial depth of the channel, this method only approximates the floodplain surface in 1949, which contributes to the overall uncertainty of the incision and incision volume calculation. Moreover, if channel widening occurred during the studied period, the final eroded volume consists of both in-channel incision process and lateral expansion. For the Belá River, calculations of the FCS eroded volume of 14 401 m³ in the control REF section can be used as an error estimation of uncertainty for this method. Another constraint is that methods are applicable in the reaches with progressive channel incision and active lateral movement with well-preserved old channel surfaces. Moreover, it does not allow the detection of sediment aggradation and incision occurring between times of imaging.

Nevertheless, the detection of floodplain elevation height is affected by the spatial accuracy of channel vectorisation and initial data referencing (Swanson et al., 2011). Especially in areas with intensive human activity, analyses need to exclude all human-made topographic objects such as embankments, terrain modification, roads, bridges and urbanised areas. The elevation model of the Belá River was cleaned from the anthropogenic object on the floodplain within the floodplain age map's extent. Still, a nondetectable object or an object with a questionable landform origin can be preserved. Several outliers in the floodplain surface height analyses (Figure 7b) above 5.5 m can be related to the construction of a small hydropower plant or postbuilding landscaping, which cannot be distinguishable from DEMs. Furthermore, the height of the FCS is affected by the depth of the flood deposits stored on the older floodplain surfaces during the study period, which should be excluded from the calculation.

6 | CONCLUSIONS

Channel incision was detected by an innovative approach involving floodplain spatial memory extracted from LiDAR data. The extreme channel incision of up to 4.05 m in the DEG section was estimated based on differentiating between the floodplain and the channel's vertical position from the period 1949–2020. Field surveys and cross-sections confirm ongoing intensive channel incisions of up to 2.5 m between 2011 and 2021. The BACI approach combined (*Pre* and *Post* state), and spatial localisation of reaches (CHAN, DEG, REF) enables identified mutual cause–effect relationships of different driver's impacts. Control sections located upstream from impacted reach are affected by channel transformation but without propagation of channel bed lowering. This pointed to the catchment scale impact on channel narrowing and local downstream drivers for channel incision. Upstream conditions, including forest recovery in the upper catchment, point to the progressive planform changes of this valuable multichannel system. Incision evidence only in the downstream part points to the direct effect of active human intervention, specifically with the commencement of channelisation works, embankment construction and gravel mining. A significant deficit of sediment in the

DEG section after the emptying of channel infill with headcut propagation is threatening the multichannel system and has led to the loss of biodiversity and rare species in the Natura 2000 protected area. By applying SfM-photogrammetry, it has been possible to identify ongoing backward incision of up to 1.39 m in the upper part of the most degraded river section and enable effective monitoring and mapping of in-channel processes. In this situation, only active management aimed at increasing sediment flux in the upper catchment area can help reduce the intensity of river degradation. However, these activities contrast with the antiflood measures declared in the lower section of the Belá River.

AUTHOR CONTRIBUTIONS

Miloš Rusnák: Conceptualisation; methodology; investigation; writing—initial draft; visualisation. **Ján Kaňuk:** Conceptualisation; investigation; writing—initial draft. **Anna Kidová:** Investigation; funding acquisition. **Milan Lehotský:** Conceptualisation; supervision; writing—reviewing and editing. **Hervé Piégay:** Conceptualisation; supervision; writing—reviewing and editing. **Ján Sládek:** Investigation; writing—initial draft. **Lukáš Michaleje:** Investigation.

ACKNOWLEDGEMENTS

The study was supported by the Science Grant Agency (VEGA) of the Ministry of the Education, Science, Research and Sport of the Slovak Republic and the Slovak Academy of Sciences [Grant Nr. 02/0016/24 and Nr. 01/0085/23]. This research was conducted within the framework of the Graduate School H2O'Lon (ANR-17-EURE-0018) of the Université de Lyon (UdL), which is part of the program “Investissements d'Avenir” run by Agence Nationale de la Recherche (ANR). The authors are grateful to the Geodesy, Cartography and Cadastre Authority of the Slovak Republic (ÚGKK SR) for providing LiDAR data. The historical aerial images were provided by the Topographic Institute in Banská Bystrica, and the orthophotos by Eurosense Slovakia, s.r.o. and the Geodetic and Cartographic Institute Bratislava (GKÚ) with the National Forest Centre (NLC). The authors would like to thank the reviewers for taking the time and effort necessary to review the manuscript. The authors sincerely appreciate all the valuable comments and suggestions that helped us improve the quality of the manuscript.

DATA AVAILABILITY STATEMENT

Orthophotomosaics of Slovakia from 2017 and LiDAR data are freely available from the Geodesy, Cartography and Cadastre Authority of the Slovak Republic website (LiDAR: https://www.geoportal.sk/en/zbgis/als_dmr/ and orthophotomosaics: <https://www.geoportal.sk/en/zbgis/orthophotomosaic/>). Orthophotomosaics (2002–2015) and historical aerial images (1949–1992) were purchased under a commercial license and are subject to restrictions. The data are available with the permission of the third party upon reasonable request to the corresponding author. UAV point cloud data are available upon request to the corresponding author from the repository of the Institute of Geography SAS.

ORCID

Miloš Rusnák  <https://orcid.org/0000-0002-4553-276X>
Hervé Piégay  <https://orcid.org/0000-0002-3864-2119>

REFERENCES

- Armaş, I., Gogoşe Nistoran, D.E., Osaci-Costache, G. & Braşoveanu, L. (2013) Morpho-dynamic evolution patterns of Subcarpathian Prahova River (Romania). *Catena*, 100, 83–99. Available from: <https://doi.org/10.1016/j.catena.2012.07.007>
- Arnaud, F., Piégay, H., Schmitt, L., Rollet, A.J., Ferrier, V. & Béal, D. (2015) Historical geomorphic analysis (1932–2011) of a by-passed river reach in process-based restoration perspectives: the Old Rhine downstream of the Kembs diversion dam (France, Germany). *Geomorphology*, 236, 163–177. Available from: <https://doi.org/10.1016/j.geomorph.2015.02.009>
- Bertalan, L., Rodrigo-Comino, J., Surian, N., Šulc Michalková, M., Kovács, Z., Szabó, S., et al. (2019) Detailed assessment of spatial and temporal variations in river channel changes and meander evolution as a preliminary work for effective floodplain management. The example of Sajó River, Hungary. *Journal of Environmental Management*, 248, 109277. Available from: <https://doi.org/10.1016/j.jenvman.2019.109277>
- Bertoldi, W., Gurnell, A.M. & Drake, N.A. (2011) The topographic signature of vegetation development along a braided river: results of a combined analysis of airborne lidar, color air photographs, and ground measurements. *Water Resources Research*, 47(6), 1–13. Available from: <https://doi.org/10.1029/2010WR010319>
- Bizzi, S., Piégay, H., Demarchi, L., van de Bund, W., Weissteiner, C.J. & Gob, F. (2019) LiDAR-based fluvial remote sensing to assess 50–100-year human-driven channel changes at a regional level: the case of the Piedmont Region, Italy. *Earth Surface Processes and Landforms*, 44(2), 471–489. Available from: <https://doi.org/10.1002/esp.4509>
- Brasington, J., Langham, J. & Rumsby, B. (2003) Methodological sensitivity of morphometric estimates of coarse fluvial sediment transport. *Geomorphology*, 53(3–4), 299–316. Available from: [https://doi.org/10.1016/S0169-555X\(02\)00320-3](https://doi.org/10.1016/S0169-555X(02)00320-3)
- Brierley, G.J. & Mum, C.P. (1997) European impacts on downstream sediment transfer and bank erosion in Cobargo catchment, New South Wales, Australia. *Catena*, 31(1–2), 119–136. Available from: [https://doi.org/10.1016/S0341-8162\(97\)00025-8](https://doi.org/10.1016/S0341-8162(97)00025-8)
- Brousse, G., Liébault, F., Arnaud-Fassetta, G., Breilh, B. & Tacon, S. (2021) Gravel replenishment and active-channel widening for braided-river restoration: the case of the Upper Drac River (France). *Science of the Total Environment*, 766, 142517. Available from: <https://doi.org/10.1016/J.SCITOTENV.2020.142517>
- Bulteau, T., Batalla, R.J., Chapron, E., Valette, P. & Piégay, H. (2022) Geomorphic effects of a run-of-the-river dam in a multi-driver context: the case of the Upper Garonne (Central Pyrenees). *Geomorphology*, 408, 108243. Available from: <https://doi.org/10.1016/j.geomorph.2022.108243>
- Calle, M., Alho, P. & Benito, G. (2017) Channel dynamics and geomorphic resilience in an ephemeral Mediterranean river affected by gravel mining. *Geomorphology*, 285, 333–346. Available from: <https://doi.org/10.1016/j.geomorph.2017.02.026>
- Calle, M., Alho, P. & Benito, G. (2018) Monitoring ephemeral river changes during floods with SfM photogrammetry. *Journal of Iberian Geology*, 44(3), 355–373. Available from: <https://doi.org/10.1007/s41513-018-0078-y>
- Calle, M., Calle, J., Alho, P. & Benito, G. (2020) Inferring sediment transfers and functional connectivity of rivers from repeat topographic surveys. *Earth Surface Processes and Landforms*, 45(3), 681–693. Available from: <https://doi.org/10.1002/ESP.4765>
- Chiriloaei, F., Rădoane, M., Perşoiu, I. & Popa, I. (2012) Late Holocene history of the Moldova River Valley, Romania. *Catena*, 93, 64–77. Available from: <https://doi.org/10.1016/j.catena.2012.01.008>
- Croke, J., Fryirs, K. & Thompson, C. (2013) Channel-floodplain connectivity during an extreme flood event: implications for sediment erosion, deposition, and delivery. *Earth Surface Processes and Landforms*, 38(12), 1444–1456. Available from: <https://doi.org/10.1002/esp.3430>
- Dietrich, J.T. (2017) Bathymetric structure-from-motion: extracting shallow stream bathymetry from multi-view stereo photogrammetry. *Earth Surface Processes and Landforms*, 42(2), 355–364. Available from: <https://doi.org/10.1002/esp.4060>
- Downs, P.W., Dusterhoff, S.R. & Sears, W.A. (2013) Reach-scale channel sensitivity to multiple human activities and natural events: lower Santa Clara River, California, USA. *Geomorphology*, 189, 121–134. Available from: <https://doi.org/10.1016/j.geomorph.2013.01.023>
- Dufour, S. & Piégay, H. (2010) Channel vertical mobility, hydrogeomorphic disturbances and understory vegetation in floodplain forests of the Ain River (France). *Géomorphologie: Relief, Processus, Environment*, 16(4), 371–386. Available from: <https://doi.org/10.4000/geomorphologie.8101>
- Dufour, S., Rinaldi, M., Piégay, H. & Michalon, A. (2015) How do river dynamics and human influences affect the landscape pattern of fluvial corridors? Lessons from the Magra River, Central–Northern Italy. *Landscape and Urban Planning*, 134, 107–118. Available from: <https://doi.org/10.1016/J.LANDURBPLAN.2014.10.007>
- Falt'an, V., Katina, S., Minár, J., Polčák, N., Bánovský, M., Mareta, M., et al. (2020) Evaluation of abiotic controls on windthrow disturbance using a generalized additive model: a case study of the Tatra National Park, Slovakia. *Forests*, 11(12), 1259. Available from: <https://doi.org/10.3390/F11121259>
- Falt'an, V., Petrovič, F., Gábor, M., Šagát, V. & Hruška, M. (2021) Mountain landscape dynamics after large wind and bark beetle disasters and subsequent logging—case studies from the Carpathians. *Remote Sensing*, 13(19), 3873. Available from: <https://doi.org/10.3390/RS13193873>
- Ferrer-Boix, C., Scorpio, V., Martín-Vide, J.P., Núñez-González, F. & Mora, D. (2023) Massive incision and outcropping of bedrock in a former braided river attributed to mining and training. *Geomorphology*, 436, 108774. Available from: <https://doi.org/10.1016/j.geomorph.2023.108774>
- Fonstad, M.A., Dietrich, J.T., Courville, B.C., Jensen, J.L. & Carbonneau, P.E. (2013) Topographic structure from motion: a new development in photogrammetric measurement. *Earth Surface Processes and Landforms*, 38(4), 421–430. Available from: <https://doi.org/10.1002/esp.3366>
- Galay, V.J. (1983) Causes of river bed degradation. *Water Resources Research*, 19(5), 1057–1090. Available from: <https://doi.org/10.1029/WR019i005p1057>
- Gorczyca, E., Krzemień, K. & Jarzyna, K. (2020) The evolution of gravel-bed rivers during the post-regulation period in the Polish Carpathians. *Watermark*, 12(1), 254. Available from: <https://doi.org/10.3390/w12010254>
- Greco, S.E., Fremier, A.K., Larsen, E.W. & Plant, R.E. (2007) A tool for tracking floodplain age land surface patterns on a large meandering river with applications for ecological planning and restoration design. *Landscape and Urban Planning*, 81(4), 354–373. Available from: <https://doi.org/10.1016/J.LANDURBPLAN.2007.01.002>
- Gross, P., Vaškovský, I. & Halouzka, R. (1979) *Geologická mapa Liptovskej kotliny [Geological map of Liptovská kotlina Basin]*. Bratislava: GUDŠ.
- Hajdukiewicz, H. & Wyźga, B. (2022) Twentieth-century development of floodplain forests in Polish Carpathian valleys: the by-product of transformation of river channels? *Science of the Total Environment*, 802, 149853. Available from: <https://doi.org/10.1016/j.scitotenv.2021.149853>
- Hajdukiewicz, M., Wyźga, B., Hajdukiewicz, H. & Mikuś, P. (2019) Photogrammetric reconstruction of changes in vertical river position using archival aerial photos: case study of the Czarny Dunajec River, Polish Carpathians. *Acta Geophysica*, 67(4), 1205–1221. Available from: <https://doi.org/10.1007/s11600-019-00307-0>
- Hajdukiewicz, H., Wyźga, B. & Zawiejska, J. (2017) Twentieth-century hydromorphological degradation of Polish Carpathian rivers. *Quaternary International*, 504, 181–194. Available from: <https://doi.org/10.1016/j.quaint.2017.12.011>
- Ham, D. & Church, M. (2012) Morphodynamics of an extended bar complex, Fraser River, British Columbia. *Earth Surface Processes and Landforms*, 37(10), 1074–1089. Available from: <https://doi.org/10.1002/esp.3231>
- Heritage, G. & Hetherington, D. (2007) Towards a protocol for laser scanning in fluvial geomorphology. *Earth Surface Processes and Landforms*, 32(1), 66–74. Available from: <https://doi.org/10.1002/esp.1375>

- James, L.A. (1991) Incision and morphologic evolution of an alluvial channel recovering from hydraulic mining sediment. *Geological Society of America Bulletin*, 103(6), 723–736. Available from: [https://doi.org/10.1130/0016-7606\(1991\)103<0723:IAMEOA>2.3.CO;2](https://doi.org/10.1130/0016-7606(1991)103<0723:IAMEOA>2.3.CO;2)
- James, L.A. (1997) Channel incision on the Lower American River, California, from streamflow gage records. *Water Resources Research*, 33(3), 485–490. Available from: <https://doi.org/10.1029/96WR03685>
- James, M.R. & Robson, S. (2012) Straightforward reconstruction of 3D surfaces and topography with a camera: accuracy and geoscience application. *Journal of Geophysical Research - Earth Surface*, 117(F3), 2011JF002289. Available from: <https://doi.org/10.1029/2011JF002289>
- Jefferson, A.J. & McGee, R.W. (2013) Channel network extent in the context of historical land use, flow generation processes, and landscape evolution in the North Carolina Piedmont. *Earth Surface Processes and Landforms*, 38(6), 601–613. Available from: <https://doi.org/10.1002/esp.3308>
- Kidová, A., Lehotský, M. & Rusnák, M. (2016) Geomorphic diversity in the braided-wandering Belá River, Slovak Carpathians, as a response to flood variability and environmental changes. *Geomorphology*, 272, 137–149. Available from: <https://doi.org/10.1016/j.geomorph.2016.01.002>
- Kidová, A., Lehotský, M. & Rusnák, M. (2017) Recent channel planform evolution of a braided-wandering river using multitemporal data and GIS (case study of the Belá River, Slovak Carpathians). *Acta Scientiarum Polonorum-Formatio Circumiectus*, 16(1), 247–259. Available from: <https://doi.org/10.15576/ASP.FC/2017.16.1.247>
- Kidová, A., Radecki-Pawlik, A., Rusnák, M. & Plesiński, K. (2021) Hydromorphological evaluation of the river training impact on a multi-thread river system (Belá River, Carpathians, Slovakia). *Scientific Reports*, 11(1), 6289. Available from: <https://doi.org/10.1038/s41598-021-85805-2>
- Klimek, K. (1987) Man's impact on fluvial processes in the Polish Western Carpathians. *Geografiska Annaler: Series A, Physical Geography*, 69(1), 221–226. Available from: <https://doi.org/10.1080/04353676.1987.11880209>
- Kondolf, G.M. (1997) PROFILE: hungry water: effects of dams and gravel mining on river channels. *Environmental Management*, 21(4), 533–551. Available from: <https://doi.org/10.1007/s002679900048>
- Kondolf, G.M., Piégay, H. & Landon, N. (2002) Channel response to increased and decreased bedload supply from land use change: contrasts between two catchments. *Geomorphology*, 45(1–2), 35–51. Available from: [https://doi.org/10.1016/S0169-555X\(01\)00188-X](https://doi.org/10.1016/S0169-555X(01)00188-X)
- Kondolf, G.M. & Swanson, M.L. (1993) Channel adjustments to reservoir construction and gravel extraction along Stony Creek, California. *Environmental Geology*, 21(4), 256–269. Available from: <https://doi.org/10.1007/BF00775916>
- Korpak, J. (2007) The influence of river training on mountain channel changes (Polish Carpathian Mountains). *Geomorphology*, 92(3–4), 166–181. Available from: <https://doi.org/10.1016/j.geomorph.2006.07.037>
- Kunca, A. (2013) Výskyt škodlivých činiteľov v lesoch Slovenska za rok 2012 a ich prognóza na rok 2013 [Occurrence of harmful agents in the forests of Slovakia in 2012 and their forecast for 2013]. Zvolen. http://www.los.sk/pdf/elab_13.pdf (Accessed 7 March 2023).
- Lach, J. & Wyźga, B. (2002) Channel incision and flow increase of the upper Wisłoka River, southern Poland, subsequent to the reafforestation of its catchment. *Earth Surface Processes and Landforms*, 27(4), 445–462. Available from: <https://doi.org/10.1002/esp.329>
- Lallias-Tacon, S., Liébault, F. & Piégay, H. (2017) Use of airborne LiDAR and historical aerial photos for characterising the history of braided river floodplain morphology and vegetation responses. *Catena*, 149(3), 742–759. Available from: <https://doi.org/10.1016/j.catena.2016.07.038>
- Liébault, F., Gomez, B., Page, M., Marden, M., Peacock, D., Richard, D., et al. (2005) Land-use change, sediment production and channel response in upland regions. *River Research and Applications*, 21(7), 739–756. Available from: <https://doi.org/10.1002/rra.880>
- Liébault, F. & Piégay, H. (2002) Causes of 20th century channel narrowing in mountain and piedmont rivers of southeastern France. *Earth Surface Processes and Landforms*, 27(4), 425–444. Available from: <https://doi.org/10.1002/esp.328>
- Liro, M. (2015) Gravel-bed channel changes upstream of a reservoir: the case of the Dunajec River upstream of the Czorsztyn Reservoir, southern Poland. *Geomorphology*, 228, 694–702. Available from: <https://doi.org/10.1016/j.geomorph.2014.10.030>
- Llena, M., Vericat, D., Martínez-Casasnovas, J.A. & Smith, M.W. (2020) Geomorphic adjustments to multi-scale disturbances in a mountain river: a century of observations. *Catena*, 192, 104584. Available from: <https://doi.org/10.1016/J.CATENA.2020.104584>
- Majerčáková, O., Škoda, P. & Danáčová, Z. (2007) Vývoj vybraných hydrologických a zrážkových charakteristík za obdobia 1961–2000 a 2001–2006 v oblasti Vysokých Tatier [The development of selected hydrological and precipitation characteristics of 1961–2000 and 2001–2006 periods in the High Tatras region]. *Meteorologický časopis*, 10, 205–210.
- Marchese, E., Scorpio, V., Fuller, I., McColl, S. & Comiti, F. (2017) Morphological changes in Alpine rivers following the end of the Little Ice Age. *Geomorphology*, 295, 811–826. Available from: <https://doi.org/10.1016/j.geomorph.2017.07.018>
- Marston, R.A., Bravard, J.P. & Green, T. (2003) Impacts of reforestation and gravel mining on the Malnant River, Haute-Savoie, French Alps. *Geomorphology*, 55(1–4), 65–74. Available from: [https://doi.org/10.1016/S0169-555X\(03\)00132-6](https://doi.org/10.1016/S0169-555X(03)00132-6)
- Marteau, B., Gibbins, C., Vericat, D. & Batalla, R.J. (2020) Geomorphological response to system-scale river rehabilitation I: sediment supply from a reconnected tributary. *River Research and Applications*, 36(8), 1488–1503. Available from: <https://doi.org/10.1002/rra.3683>
- Marteau, B., Michel, K. & Piégay, H. (2022) Can gravel augmentation restore thermal functions in gravel-bed rivers? A need to assess success within a trajectory-based before–after control–impact framework. *Hydrological Processes*, 36(2), e14480. Available from: <https://doi.org/10.1002/hyp.14480>
- Marteau, B., Vericat, D., Gibbins, C., Batalla, R.J. & Green, D.R. (2017) Application of structure-from-motion photogrammetry to river restoration. *Earth Surface Processes and Landforms*, 42(3), 503–515. Available from: <https://doi.org/10.1002/ESP.4086>
- Martin, Y. & Church, M. (1995) Bed-material transport estimated from channel surveys: Vedder River, British Columbia. *Earth Surface Processes and Landforms*, 20(4), 347–361. Available from: <https://doi.org/10.1002/esp.3290200405>
- Martín-Vide, J.P., Ferrer-Boix, C. & Ollero, A. (2010) Incision due to gravel mining: modeling a case study from the Gállego River, Spain. *Geomorphology*, 117(3–4), 261–271. Available from: <https://doi.org/10.1016/j.geomorph.2009.01.019>
- Michalková, M., Piégay, H., Kondolf, G.M. & Greco, S.E. (2011) Lateral erosion of the Sacramento River, California (1942–1999), and responses of channel and floodplain lake to human influences. *Earth Surface Processes and Landforms*, 36(2), 257–272. Available from: <https://doi.org/10.1002/esp.2106>
- Miřijovský, J. & Langhammer, J. (2015) Multitemporal monitoring of the morphodynamics of a mid-mountain stream using UAS photogrammetry. *Remote Sensing*, 7(7), 8586–8609. Available from: <https://doi.org/10.3390/rs70708586>
- Nemčok, J., et al. (1994) *Geologická mapa Tatier [Geological map of the Tatra Mountains]*. Bratislava: GUDŠ.
- Nikolov, C., Konôpka, B., Kajba, M., Galko, J., Kunca, A. & Janský, L. (2014) Post-disaster forest management and bark beetle outbreak in Tatra National Park, Slovakia. *Mountain Research and Development*, 34(4), 326–335. Available from: <https://doi.org/10.1659/MRD-JOURNAL-D-13-00017.1>
- Ollero, A. (2010) Channel changes and floodplain management in the meandering middle Ebro River, Spain. *Geomorphology*, 117(3–4), 247–260. Available from: <https://doi.org/10.1016/J.GEOMORPH.2009.01.015>
- Peiry, J.L. (1987) Channel degradation in the middle Arve river, France. *Regulated Rivers: Research & Management*, 1(2), 183–188. Available from: <https://doi.org/10.1002/RRR.3450010208>
- Perşoiu, I. & Rădoane, M. (2011) Spatial and temporal controls on historical channel responses—study of an atypical case: Someşu Mic River,

- Romania. *Earth Surface Processes and Landforms*, 36(10), 1391–1409. Available from: <https://doi.org/10.1002/esp.2169>
- Petit, F., Poinart, D. & Bravard, J.P. (1996) Channel incision, gravel mining and bedload transport in the Rhône river upstream of Lyon, France (“canal de Miribel”). *Catena*, 26(3–4), 209–226. Available from: [https://doi.org/10.1016/0341-8162\(95\)00047-X](https://doi.org/10.1016/0341-8162(95)00047-X)
- Price, K. & Leigh, D.S. (2006) Morphological and sedimentological responses of streams to human impact in the southern Blue Ridge Mountains, USA. *Geomorphology*, 78(1–2), 142–160. Available from: <https://doi.org/10.1016/j.geomorph.2006.01.022>
- Rădoane, M., Obreja, F., Cristea, I. & Mihailă, D. (2013) Changes in the channel-bed level of the eastern Carpathian rivers: climatic vs. human control over the last 50 years. *Geomorphology*, 193, 91–111. Available from: <https://doi.org/10.1016/j.geomorph.2013.04.008>
- Rădoane, M., Pandi, G. & Rădoane, N. (2010) Contemporary bed elevation changes from the Eastern Carpathians. *Carpathian Journal of Earth and Environmental Sciences*, 5, 49–60.
- Rinaldi, M. (2003) Recent channel adjustment in alluvial rivers of Tuscany, central Italy. *Earth Surface Processes and Landforms*, 28(6), 587–608. Available from: <https://doi.org/10.1002/esp.464>
- Rinaldi, M. & Simon, A. (1998) Bed-level adjustments in the Arno River, central Italy. *Geomorphology*, 22(1), 57–71. Available from: [https://doi.org/10.1016/S0169-555X\(97\)00054-8](https://doi.org/10.1016/S0169-555X(97)00054-8)
- Rinaldi, M., Wyzga, B. & Surian, N. (2005) Sediment mining in alluvial channels: physical effects and management perspectives. *River Research and Applications*, 21(7), 805–828. Available from: <https://doi.org/10.1002/rra.884>
- Roux, C., Alber, A., Bertrand, M., Vaudor, L. & Piégay, H. (2015) “FluvialCorridor”: a new ArcGIS toolbox package for multiscale riverscape exploration. *Geomorphology*, 242, 29–37. Available from: <https://doi.org/10.1016/j.geomorph.2014.04.018>
- Rovira, A., Batalla, R.J. & Sala, M. (2005) Response of a river sediment budget after historical gravel mining (the lower Tordera, NE Spain). *River Research and Applications*, 21(7), 829–847. Available from: <https://doi.org/10.1002/rra.885>
- Rusnák, M., Kaňuk, J., Kidová, A., Šašák, J., Lehotský, M., Pöpl, R., et al. (2020) Channel and cut-bluff failure connectivity in a river system: case study of the braided-wandering Belá River, Western Carpathians, Slovakia. *Science of the Total Environment*, 733, 139409. Available from: <https://doi.org/10.1016/j.scitotenv.2020.139409>
- Rusnák, M., Lehotský, M. & Kidová, A. (2016) Channel migration inferred from aerial photographs, its timing and environmental consequences as responses to floods: a case study of the meandering Topľa River, Slovak Carpathians. *Moravian Geographical Reports*, 24(3), 32–43. Available from: <https://doi.org/10.1515/mgr-2016-0015>
- Rusnák, M., Sládek, J. & Kidová, A. (2018) Využitie UAV technológie pre klasifikáciu a mapovanie krajiny vo fluvialnej geomorfológii. *Geografický časopis*, 70(2), 141–160. Available from: <https://doi.org/10.31577/geogrcas.2018.70.2.08>
- Rusnák, M., Sládek, J., Kidová, A. & Lehotský, M. (2018) Template for high-resolution river landscape mapping using UAV technology. *Measurement*, 115, 139–151. Available from: <https://doi.org/10.1016/j.measurement.2017.10.023>
- Šamajová, L. & Hók, J. (2018) Hustota horninových komplexov Západných Karpát na území Slovenska [Densities of rock formations of the Western Carpathians in the territory of Slovakia]. *Geologické práce, Správy*, 132, 31–52.
- Scorpio, V., Aucelli, P.P.C., Giano, S.I., Pisano, L., Robustelli, G., Roskopf, C.M., et al. (2015) River channel adjustments in Southern Italy over the past 150 years and implications for channel recovery. *Geomorphology*, 251, 77–90. Available from: <https://doi.org/10.1016/j.geomorph.2015.07.008>
- Scorpio, V. & Piégay, H. (2021) Is afforestation a driver of change in Italian rivers within the Anthropocene era? *Catena*, 198, 105031. Available from: <https://doi.org/10.1016/J.CATENA.2020.105031>
- Scorpio, V., Zen, S., Bertoldi, W., Surian, N., Mastrorunzio, M., Dai Prá, E., et al. (2018) Channelization of a large Alpine river: what is left of its original morphodynamics? *Earth Surface Processes and Landforms*, 43(5), 1044–1062. Available from: <https://doi.org/10.1002/esp.4303>
- Simon, A. & Hupp, C.R. (1987) Geomorphic and vegetative recovery processes along modified Tennessee streams: an interdisciplinary approach to distributed fluvial systems. *International Association of Hydrological Sciences*, 167, 251–262.
- Simon, A. & Rinaldi, M. (2006) Disturbance, stream incision, and channel evolution: the roles of excess transport capacity and boundary materials in controlling channel response. *Geomorphology*, 79(3–4), 361–383. Available from: <https://doi.org/10.1016/j.geomorph.2006.06.037>
- Škarpich, V., Galia, T. & Hradecký, J. (2016) Channel bed adjustment to over bankfull discharge magnitudes of the flysch gravel-bed stream—case study from the channelized reach of the Olše River (Czech Republic). *Zeitschrift für Geomorphologie*, 60(4), 327–341. Available from: <https://doi.org/10.1127/zfg/2016/0395>
- Škarpich, V., Hradecký, J. & Dušek, R. (2013) Complex transformation of the geomorphic regime of channels in the forefield of the Moravskoslezské Beskydy Mts.: case study of the Morávka River (Czech Republic). *Catena*, 111, 25–40. Available from: <https://doi.org/10.1016/j.catena.2013.06.028>
- Škarpich, V., Kašpárek, Z., Galia, T. & Hradecký, J. (2016) Antropogenní impakt a jeho odezva v morfologii koryt beskydských štěrkonosných toků: Příkladová studie řeky Ostravice, Česko. *Geografie-Sborník CGS*, 121(1), 99–120. Available from: <https://doi.org/10.37040/geografie2016121010099>
- Škarpich, V., Macurová, T., Galia, T., Ruman, S. & Hradecký, J. (2020) Degradation of multi-thread gravel-bed rivers in medium-high mountain settings: Quantitative analysis and possible solutions. *Ecological Engineering*, 148, 105795. Available from: <https://doi.org/10.1016/j.ecoleng.2020.105795>
- Surian, N. (1999) Channel changes due to river regulation: the case of the Piave River, Italy. *Earth Surface Processes and Landforms*, 24(12), 1135–1151. Available from: [https://doi.org/10.1002/\(SICI\)1096-9837\(199911\)24:12<1135::AID-ESP40>3.0.CO;2-F](https://doi.org/10.1002/(SICI)1096-9837(199911)24:12<1135::AID-ESP40>3.0.CO;2-F)
- Surian, N. & Cissotto, A. (2007) Channel adjustments, bedload transport and sediment sources in a gravel-bed river, Brenta River, Italy. *Earth Surface Processes and Landforms*, 32(11), 1641–1656. Available from: <https://doi.org/10.1002/esp.1591>
- Surian, N. & Rinaldi, M. (2003) Morphological response to river engineering and management in alluvial channels in Italy. *Geomorphology*, 50(4), 307–326. Available from: [https://doi.org/10.1016/S0169-555X\(02\)00219-2](https://doi.org/10.1016/S0169-555X(02)00219-2)
- Surian, N., Ziliani, L., Comiti, F., Lenzi, M.A. & Mao, L. (2009) Channel adjustments and alteration of sediment fluxes in gravel-bed rivers of North-Eastern Italy: potentials and limitations for channel recovery. *River Research and Applications*, 25(5), 551–567. Available from: <https://doi.org/10.1002/rra.1231>
- Swanson, B.J., Meyer, G.A. & Coonrod, J.E. (2011) Historical channel narrowing along the Rio Grande near Albuquerque, New Mexico in response to peak discharge reductions and engineering: magnitude and uncertainty of change from air photo measurements. *Earth Surface Processes and Landforms*, 36(7), 885–900. Available from: <https://doi.org/10.1002/esp.2119>
- Wheaton, J.M., Brasington, J., Darby, S.E., Kasprak, A., Sear, D. & Vericat, D. (2013) Morphodynamic signatures of braiding mechanisms as expressed through change in sediment storage in a gravel-bed river. *Journal of Geophysical Research - Earth Surface*, 118(2), 759–779. Available from: <https://doi.org/10.1002/jgrf.20060>
- Wheaton, J.M., Brasington, J., Darby, S.E. & Sear, D.A. (2009) Accounting for uncertainty in DEMs from repeat topographic surveys: improved sediment budgets. *Earth Surface Processes and Landforms*, 35(2), 136–156. Available from: <https://doi.org/10.1002/esp.1886>
- Wiejaczka, L. & Kijowska-Strugała, M. (2015) Dynamics of the channel beds level in mountain rivers in the light of the minimum water stages analysis. *Carpathian Journal of Earth and Environmental Sciences*, 10(4), 105–112.
- Williams, R.D., Brasington, J., Vericat, D. & Hicks, D.M. (2014) Hyperscale terrain modelling of braided rivers: fusing mobile terrestrial laser scanning and optical bathymetric mapping. *Earth Surface Processes*

- and *Landforms*, 39(2), 167–183. Available from: <https://doi.org/10.1002/esp.3437>
- Woodget, A.S., Dietrich, J.T. & Wilson, R.T. (2019) Quantifying below-water fluvial geomorphic change: the implications of refraction correction, water surface elevations, and spatially variable error. *Remote Sensing*, 11(20), 2415. Available from: <https://doi.org/10.3390/rs11202415>
- Wyźga, B. (1991) Present-day downcutting of the Raba River channel (western Carpathians, Poland) and its environmental effects. *Catena*, 18(6), 551–566. Available from: [https://doi.org/10.1016/0341-8162\(91\)90038-Y](https://doi.org/10.1016/0341-8162(91)90038-Y)
- Wyźga, B. (1993) River response to channel regulation: case study of the Raba river, Carpathians, Poland. *Earth Surface Processes and Landforms*, 18(6), 541–556. Available from: <https://doi.org/10.1002/esp.3290180607>
- Wyźga, B. (2001) Impact of the channelization-induced incision of the Skawa and Wisłoka Rivers, southern Poland, on the conditions of overbank deposition. *Regulated Rivers: Research & Management*, 17(1), 85–100. Available from: [https://doi.org/10.1002/1099-1646\(200101/02\)17:1<85::AID-RRR605>3.0.CO;2-U](https://doi.org/10.1002/1099-1646(200101/02)17:1<85::AID-RRR605>3.0.CO;2-U)
- Wyźga, B., Zawiejska, J. & Hajdukiewicz, H. (2016) Multi-thread rivers in the Polish Carpathians: occurrence, decline and possibilities of restoration. *Quaternary International*, 415, 344–356. Available from: <https://doi.org/10.1016/j.quaint.2015.05.015>
- Wyźga, B., Zawiejska, J. & Radecki-Pawlik, A. (2016) Impact of channel incision on the hydraulics of flood flows: examples from Polish Carpathian rivers. *Geomorphology*, 272, 10–20. Available from: <https://doi.org/10.1016/j.geomorph.2015.05.017>
- Zawiejska, J. & Wyźga, B. (2010) Twentieth-century channel change on the Dunajec River, southern Poland: patterns, causes and controls. *Geomorphology*, 117(3–4), 234–246. Available from: <https://doi.org/10.1016/j.geomorph.2009.01.014>
- Ziliani, L. & Surian, N. (2012) Evolutionary trajectory of channel morphology and controlling factors in a large gravel-bed river. *Geomorphology*, 173–174, 104–117. Available from: <https://doi.org/10.1016/j.geomorph.2012.06.001>

SUPPORTING INFORMATION

Additional supporting information can be found online in the Supporting Information section at the end of this article.

How to cite this article: Rusnák, M., Kaňuk, J., Kídová, A., Lehotský, M., Piégay, H., Sládek, J. et al. (2024) Inferring channel incision in gravel-bed rivers: Integrating LiDAR data, historical aerial photographs and drone-based SfM topo-bathymetry. *Earth Surface Processes and Landforms*, 1–23. Available from: <https://doi.org/10.1002/esp.5840>